Impacts of aerosol-radiation interaction on meteorological forecast over northern China by offline coupling the WRF-Chem simulated AOD into WRF: a case study during a heavy pollution event

Yang Yang[1], Min Chen[1], Xiujuan Zhao[1*], Dan Chen[1*], Shuiyong Fan[1],
and Shaukat Ali[2]

1 Institute of Urban Meteorology, China Meteorological Administration, Beijing 100089, China

2 Global Change Impact Studies Centre, Ministry of Climate Change, Islamabad 44000, Pakistan

Abstract

To facilitate the future inclusion of aerosol-radiation interactions in the regional operational Numerical Weather Prediction (NWP) system – RMAPS-ST (adapted from Weather Research and Forecasting, WRF) at the Institute of Urban Meteorology (IUM), China Meteorological Administration (CMA), the impacts of aerosol-radiation interactions on the forecast of surface radiation and meteorological parameters during a heavy pollution event (December 6th -10th, 2015) over northern China were investigated. The aerosol information was simulated by RMAPS-Chem (adapted from WRF model coupled with Chemistry, WRF-Chem) and then offline-coupled into Rapid Radiative Transfer Model for General Circulation Models (RRTMG) radiation scheme of WRF to enable the aerosol-radiation feedback in the forecast. To ensure the accuracy of high-frequency (hourly) updated aerosol optical depth (AOD) field, the temporal and spatial variations of simulated AOD and aerosol extinction coefficient at 550nm were evaluated against in-situ and satellite observations. Comparisons with in-situ and Moderate Resolution Imaging Spectroradiometer (MODIS), AErosol Robotic NETwork (AERONET), and Cloud-Aerosol Lidar and Infrared Pathfinder Satellite Observation (CALIPSO) satellite observations showed that the model could reproduce and spatial and vertical distribution as well as the temporal variation the of polluted episode. Further comparison of $PM_{2.5}$ with in-situ observation showed WRF-Chem reasonably captured the $PM_{2.5}$ field in terms of spatial distribution and magnitude, with the correlation coefficients of 0.85, 0.89, 0.76, 0.92 and 0.77 at Beijing, Shijiazhuang, Tianjin, Hebei and Henan, respectively. Forecasts with/without the aerosol information were conducted further, and the differences of surface radiation, energy budget, and meteorological parameters were evaluated against surface and sounding observations. The offline-coupling simulation (with aerosol-radiation interaction active) showed a remarkable decrease of downward shortwave (SW) radiation reaching surface, thus helping to reduce the overestimated SW radiation during daytime. The simulated surface radiation budget was also improved, with the biases of net surface radiation decreased by 85.3%, 50.0%, 35.4%, and 44.1% during daytime at Beijing, Tianjin, Taiyuan and Jinan respectively, accompanied by the reduction of sensible (16.1 W m^{-2}, 18.5%) and latent (6.8 W m^{-2}, 13.4%) heat fluxes emitted by the surface at noon-time. In addition, the cooling of 2-m temperature (~0.40 °C) and the decrease of horizontal wind speed near surface (~0.08 m s^{-1}) caused by the aerosol-radiation interaction over northern China helped to reduce the bias by ~73.9% and ~7.8% respectively, particularly during daytime. Further comparisons indicated that the simulation implemented AOD could better capture the vertical structure of atmospheric wind. Accompanied with the lower planetary boundary layer and the increased atmospheric stability, both U and V wind at 850hPa showed the convergence which were unfavorable for pollutants dispersion. Since RMPAS-ST provides meteorological initial condition for RMAPS-Chem, the changes of meteorology introduced by aerosol-radiation interaction would routinely impact the simulations of pollutants. These results demonstrated the profound influence of aerosol-radiation interactions on the improvement of predictive accuracy and the potential prospects to offline couple near-real-time aerosol information in regional RMAPS-ST NWP in northern China.

Key words: Aerosol-radiation interactions, offline-coupling, WRF, northern China, pollution

1. Introduction

Aerosol-radiation interactions modify the radiative energy budget of the earth-atmosphere system through the interaction between aerosols and solar radiation by scattering and absorbing mechanism as well as the absorption and emitting of thermal radiation (Ramanathan et al., 2001; Yu et al., 2006). The aerosol-radiation interaction may cool or heat the earth-atmosphere system, alter surface and atmospheric radiation and temperature structure on regional and global climate, which have been widely reported and studied (Hansen et al., 1997; Ramanathan et al., 2001; Kaufman et al., 2002; Liao et al., 2006; Zhang et al., 2010; Ghan et al., 2012; Yang et al., 2017a). Considering the lifetime of most aerosol particles and their locally uneven distribution, as well as their high dependence on emission sources and local meteorological conditions for dispersion (Rodwell and Jung, 2008; Liu et al., 2012; Liao et al, 2015), the impacts of episodic aerosol events over regional areas are worthy of more concerns (Cheng et al., 2017; Zheng et al., 2019).

With substantial aerosol loading, aerosol particles have significant influences on meteorology, and many endeavors by both field experiments and numerical models have been devoted to study the impacts of aerosol-radiation interaction on meteorological fields, including surface solar radiation, planetary boundary layer (PBL), atmospheric heating rate, atmospheric stability (Hansen et al., 1997; Ackerman et al., 2000; Quan et al., 2014; Yang et al., 2017b; Wang et al., 2018), cloud formation due to thermodynamic changes, and further the onset or reduction of precipitation systems (Grell et al., 2011; Guo et al., 2016). For instance, in worldwide, the simulations with Weather Research and Forecasting (WRF) model coupled with Chemistry (WRF-Chem) showed that by purely taking into account the aerosol-radiation interactions, aerosols may reduce incoming solar radiation by up to −9% (−16%) and 2-m temperatures by up to 0.16°C (0.37°C) in January (July) over the continental U.S. (Zhang et al., 2010) , affect meso-scale convection system owing to thermodynamic changes over Atlantic Ocean during Saharan dust eruption period (Chen et al., 2017), and lead to the distinct changes in precipitation due to the changes in temperature profile and stabilities induced by the aerosol-radiation interaction over Eastern China (Huang et al., 2016).

Northern China is experiencing heavy air pollution in past two decades, with particle matter (PM) being the primary pollutant, particularly during wintertime (Chan and Yao, 2008; Zhang et al., 2015; Zhao et al., 2019) due to the combination of high primary and precursor emissions and frequent stable meteorological conditions in this area (Elser et al., 2016; Zhang et al, 2018). The effects of aerosol-radiation interaction on meteorology were expected to be much more significant over northern China. Applying WRF and Community Multi-scale Air Quality Model (CMAQ) system (WRF-CMAQ), Wang et al. (2014) and Sekiguchi et al. (2018) reported a 53% reduction in solar radiation reaching surface and ~100m decrease of planetary boundary layer height (PBLH) in response to the presence of aerosols during a severe winter haze episode in China. Wang et al. (2015a, b) used the online chemical weather forecasting mode Global/Regional Assimilation and PrEdiction System/ Chinese Unified Atmospheric Chemistry Environment (GRAPES/CUACE) and illustrated that the solar radiation at ground decreased by 15% in Beijing–TianJin–Hebei, China, and its near surroundings, accompanied by the decrease in turbulence diffusion of about 52% and a decrease in PBLH of about 33 % during a haze episode of summertime in 2008.

Considering the significant influence of the aerosol-radiation interaction on meteorological forecasts as illustrated in many studies (Kaufman et al., 2002; Zhang et al., 2010), several weather forecast centers are conducting research to facilitate the inclusion of more complex aerosol information in operational numerical weather prediction (NWP) models. For example, Rodwell and Jung (2008) showed the local medium-range forecast skills were improved due to the application of new climatological aerosol distribution in European Centre for Medium-Range Weather Forecasts (ECMWF). Recently, a positive impact up to a 48h lead time on the 2m temperature and forecasts of surface radiative fluxes were reported in ECMWF by applying the prognostic aerosols compared to the monthly climatological aerosol (Rémy et al., 2015). Toll et al. (2016) found that the inclusion of aerosol effects in NWP system was beneficial to the accuracy of simulated radiative fluxes, temperature and humidity in the lower troposphere over Europe. In addition, it was shown that the quality of weather forecasts at UK MET office can be further advanced when the real-time aerosol distribution rather than climatological distribution was included, with the decreased bias of downward SW at surface (-2.79 W m^{-2} vs. -5.30 W m^{-2}) and the mean sea-level pressure (0.71hPa vs. 0.80hPa) (Mulcahy et al., 2014; Toll et al., 2015). For these research serving for operational NWP systems, both online and offline approaches (that aerosol information were simulated by separate chemistry system and then offline coupled to NWP model) were widely used.

In most previous research-targeted modeling studies over northern China, the aerosol-radiation interaction has been widely assessedin online-coupled meteorology-chemistry models, which might not be practical for NWP purpose. Considering aerosol particles differ by morphology, size and chemical composition, therefore, the numerical treatment of aerosol particles in atmospheric models needs sophisticated method and considerable simplifications, which may bring in more assumptions and uncertainties in online coupling (Baklanov et al., 2014). Moreover, the online simulations require quite high computational costs and could not meet the requirement of efficiency for operational NWP. Grell and Baklanov (2011) illustrated that the offline approach could generate to almost identical results compared to online simulation with the offline-coupling intervals about 0.5-1h. Thus, the computational-economic offline simulation provides a feasible and computationally less demanding approach to include the aerosol-radiation interaction in an operational NWP system. Péré et al. (2011) adopted an offline-coupling between the chemistry-transport model CHIMERE and WRF to study the radiative forcing of high load aerosols during the heat wave of summer in 2003 over Western Europe. Wang et al. (2018) offline implemented the daily AOD from Moderate Resolution Imaging Spectroradiometer (MODIS) to WRF during a heavy winter pollution at Beijing to study the effect of aerosols on boundary layer. Still, there have been few studies that adopted offline simulation to investigate the impacts of aerosol-radiation interactions over northern China in an NWP system. At Institute of Urban Meteorology, regional operational NWP system–RMAPS-ST (adapted from WRF) and regional air quality model–RMPSA-Chem (adapted from WRF-Chem) were applied operationally. In this study, we investigate the radiative effects of aerosols and their feedbacks on weather forecasting over northern China during a polluted event occurred in winter of 2015, and further potential impacts of changed meteorology to the transport and dissipation of pollution. The simulations were in the configurations of the two systems, aiming at presenting the offline-coupling of the high-frequent real-time aerosol distribution simulated by WRF-Chem and WRF, and evaluating the potential effects of aerosol-radiation interactions on the forecast skills in the RMAPS-ST system for future applications.

The remainder of the paper is organized as follows. Section 2 presents the model configuration and experimental design. In section 3, the model's capabilities in capturing and forecasting the pollution episode are validated with observations first, and impacts of aerosol-radiation interactions on meteorological forecasting over northern China are analyzed further. The final section provides the concluding remarks.

2. Model description and experimental design

WRF is a state-of-the-art atmospheric modeling system designed for both meteorological research and NWP. The WRF version 3.8.1 released in August, 2016 was used in this study for a domain covering the northern China with a horizontal resolulation of 9km (222×201 grid points, Fig. 1a), and for 50 vertical levels. The lateral boundary condications (BCs) and initial conditions (ICs) for meteorological variables are provided by the forecast of ECMWF. The major physical schemes include the Assymetric Convective Model Version 2 (ACM2) PBL scheme (Pleim, 2007), the Thompson microphysics without aerosol-aware option (Thompson et al., 2008), the Kain-Fritsch cumulus parameterization (Kain, 2004), and the National Center for Environmental Prediction, Oregon State University, Air Force, and Hydrologic Research Lab's (NOAH) land-surface module (Chen and Dudhia, 2001; Ek et al., 2003). The landuse data have been reprocessed, with a higher accuracy and finer classification for urban areas (Zhang et al., 2013) and the urban canopy model (UCM) was not actived.

The shortwave and longwave radiation scheme is the Rapid Radiative Transfer Model for General Circulation Models (RRTMG) (Iacono et al., 2008). The RRTMG scheme is a new version of RRTM added in Version 3.1, and includes the Monte Carlo Independent Column Approximation (MCICA) method of random cloud overlap. A recent intercomparison study showed that the RRTMG had relativlely smaller mean errors in solar flux at the surface and the top of the atmosphere

(Oreopoulos et al., 2012) and was considered as recommended WRF configuration for air quality modeling (Rogers et al., 2013). The RRTMG scheme is capable to include the climatological aerosol data with spatial and temporal variations or an external time varing 3D aerosol input through the option of AER_OPT (Ruiz-Arias et al., 2014). In the present study, the real-time hourly aerosol optical depth (AOD) at 550nm from external files was input into WRF following the second approach. The AOD at 550nm was calculated as the vertical integral of extinction coefficients at 550nm from WRF-Chem simulation.

WRF-Chem version 3.3.1 was applied in this study, and the horizontal resolution was 9 km, with 222×201 grid points covering northern China, which was the same configurion of WRF mentioned above. WRF-Chem simulates the formation, transformation and transport processes of both primary and secondary atmospheric pollutants, including gases and PM species (Zhao et al., 2019). Physical parameterizations included single-layer Urban Canopy Model, Noah land-surface, Yonsei University (YSU) PBL, Grell-Devenyi ensemble convection, Thompson microphysics, and RRTM longwave and Goddard shortwave radiation (Chen and Dudhia, 2001; Hong et al., 2006; Grell and Dévényi, 2002; Thompson et al., 2008; Mlawer et al., 1997; Chou and Suarez, 1999). Carbon bond mechanism Z (CBMZ) including comprehensive reactions and alterable scenarios were used as the gas-phase mechanism. Model for Simulating Aerosol Interactions and Chemistry (MOSAIC) are used with four size bins (Zaveri and Peters, 1999). Anthropogenic emission data were from the MEIC (2012) inventory (http://www.meicmodel.org/) with a resolution of 0.1 °×0.1 °. Meteorological ICs and BCs were obtained from the Final Analysis data (FNL) with a resolution of 1.0 °×1.0 ° from the National Centers for Environmental Prediction (NCEP). To generate aerosol fields for study period (Dec. 2nd-11th), 9-days WRF-Chem simulations from Dec. 2nd were conducted using prescribed idealized profiles as ICs and BCs for chemical species.

To estimate the aerosol radiative forcing and its feedbacks on meteorological fields, two sets of 24-hour WRF forecasts were conducted at 00UTC from 2nd-10th December 2015. The only difference between the two sets of forecasts is whether the aerosol radiative feedback is activated (Aero, with WRF-Chem simulated hourly AOD fields as input fields) or not (NoAero, no aerosol included), and other schemes remained the same. It is noted that the aerosol-cloud interactions were not included in the study.

The sites of observations over simulated domain and northern China plain (NCP, purple box in Fig. 1a) were shown in Fig. 1. The 550nm AOD retrievals from Level 2 of MODIS sensors onboard polar orbiting satellites Terra and Aqua satellites were adopted to evaluate the spatial distribution of modeled AOD. The vertical distribution of aerosol extinction coefficient at 550nm were compared with that from Cloud-Aerosol Lidar and Infrared Pathfinder Satellite Observations (CALIPSO) satellite. Moreover, three sites of AErosol Robotic NETwork (AERONET) were used to validate the simulation (black dots in Fig. 1b), and the observed AOD obtained from observation at the Institute of Atmospheric Physics (IAP), Chinese Academy of Sciences (39°58′ 28″ N, 116°22′ 16″ E) in Beijing city (blue dot in Fig. 1b) was also included as supplementary. The hourly observed $PM_{2.5}$ concentrations of total 813/332 monitoring stations over the study domain/NCP were from the released data by the China National Environmental Monitoring Centre (http://106.37.208.233:20035/, colored dots in Fig. 3a). For given cities (dots in Fig. 1a), hourly $PM_{2.5}$ concentration was represented by the average of data from all monitoring sites located in the city. Simulated meteorological variables including 2-m temperature and wind speed at 10m were evaluated using in-situ observations from National Meteorological Information Center (http://data.cma.cn/data/cdcindex.html) of China Meteorological Administration (CMA, dots in Fig. 8a). The radiations were observed at IAP and in-situ stations of CMA (shown as triangles in Fig. 1a). The vertical observation of atmospheric wind speed from sounding were also used (circles in Fig. 1a). The variables, sources, numbers of sites in the domain and NCP and the frequency of chemical and meteorological observations were also listed in Table 1.

3. Results

3.1 Evaluation of AOD and $PM_{2.5}$ simulated by WRF-Chem

Before the offline-coupling of the WRF-Chem simulated hourly AOD to meteorological model WRF, we first validated the simulated AOD and ensured the model’s capability to reproduce the features of the aerosol field. Figure 2 shows the spatial distribution of modeled AOD and AOD from MODIS Terra and Aqua. It was seen that WRF-Chem is capable to capture the AOD spatial distribution and also reproduced the transport paths during the event. The simulated high-valued AOD located in Henan on Dec. 6th, then the center moved to Hebei and Beijing on 7th and shifted to northeast areas afterwards. The variations of simulated AOD were in consistent with both Terra and Aqua with slightly overestimated peak value of AOD. In particular, the simulated shifting of AOD center to northeast areas was also observed in Aqua (Fig. 2r-s). To further verify the vertical distribution of aerosol extinction coefficient, Fig. 3 displayed the vertical distribution of simulated 550nm aerosol extinction coefficient compared to those from CALIPSO. Four cross sections along CALIPSO paths on 6th to 9th December were shown. The results indicated that the model could generally reproduce the vertical distribution of extinction coefficients at 550nm in terms of comparable magnitude with those from CALIPSO, particularly on 6th, 7th and 9th, December. However, CALIPSO showed more high values at lower altitude (below 1km) that model failed to capture; the inconsistency may be associated with both CALIPSO retrieval uncertainties at the low altitude and the model itself. Figure 4 further displayed the temporal variation of simulated AOD at 550nm (blue solid) at four sites, in comparison with three AERONET stations (black circles in Figs. 4a-c) and IAP site (black circles in Fig. 4d) for the period during 3rd to 11th December, 2015 (local time, LT). As shown in blue solids in Fig. 4a, the simulated AOD increased since 6th Dec. and reached the peak value of 9 on

7th, and the high AOD value maintained until 9th and reached the second peak. The second peak was also observed from AERONET though most of them were missing during the pollution event. The temporal variations of AOD at Beijing-CMA and IAP (Figs. 4b and d) were similar to those at Beijing station (Fig. 4a). Meanwhile, the simulated AOD at Xianghe (Fig. 4c) was relatively lower than those at other stations.

Considering that the aerosol extinction was mainly attributed to scattering and absorption of solar radiation by $PM_{2.5}$ and their hygroscopic growth with relative humidity (Cheng et al., 2006), next we compared the simulated $PM_{2.5}$ concentrations with corresponding in-situ observation over the model domain. As shown in Fig. 5, the simulated and observed pollution were both initiated over Henan province on 6th, further intensified and shifted northward afterwards. The polluted center located over south of Hebei province and maintained until 10th, with the maximum $PM_{2.5}$ concentration exceeding 440μg m^{-3}. The results indicated that WRF-Chem could well capture the spatial features of $PM_{2.5}$ and its temporal variation, in spite of the slight discrepancy of the center position during 9th and 10th. Figure 6 displayed the mean bias, root mean square error (RMSE), and correlation coefficient during the heavy pollution and relatively cleaner periods. It was seen that the biases of $PM_{2.5}$ were generally less than 40 μg m^{-3} with the correlation coefficient exceeding 0.8 during clean period (Fig. 6a-c). Compared with clean period, the bias and RMSE were generally larger during polluted period (Fig. 6d-f). The $PM_{2.5}$ concentrations over most areas of the domain were underestimated with the maximum bias exceeding 160μg m^{-3}. Overall, the correlation coefficient was generally higher than 0.4 in northern China during the polluted period, particularly over Beijing with the correlation coefficient reaching 0.8.

To further assess the temporal evolutions of the pollution, the simulated $PM_{2.5}$ concentrations at three major cities (Beijing, Shijiazhuang and Tianjin, shown as black dots in Fig. 1a) and two provinces (Hebei and Henan) in northern China were compared with observation as shown in Fig. 7. It showed that the hourly variations of $PM_{2.5}$ concentration, including the occurrence of several high peaks at the three cities, as well as the gradual accumulation of pollution in Hebei and Henan could be reasonably reproduced by WRF-Chem. The correlation coefficients (R) between simulation and observation at Beijing, Shijiazhuang, Tianjin, Hebei and Henan were 0.85, 0.89, 0.76, 0.92 and 0.77 respectively. It should be noted that there exits slight overestimation (underestimation) of the peak magnitude during 9th to 10th at Beijing and Shijiazhuang (Tianjin, Hebei and Henan); the overestimation in Beijing and Shijiazhuang is possibly associated with the frequent emission changes caused by emission-control-measures in reality which are not dynamically updated in the model; the underestimation is more related with the deficiency of model skills, such as missing heterogeneous reaction paths in the chemistry scheme.

3.2 Aerosol effects on meteorological simulations

In this section, the influences of aerosol-radiation interaction on the spatial and temporal variations of radiation and energy budget simulated by WRF model were analyzed, and their impacts on the forecasts of meteorological fields were discussed further.

3.2.1 Aerosol impacts on simulations of radiative forcing and heat fluxes

To illustrate the impacts of aerosol-radiation interaction on the forecasts of radiation during the pollution event, the simulated surface downward SW radiation and net radiation at Beijing, Tianjin, Taiyuan and Jinan, as denoted by the triangles in Fig. 1a, were compared with observations in Fig. 8. To show the relationship with aerosol, the time series of AOD for Dec. 3th -11th were overlaid as gray shadings in Fig. 8. During the clean stage with quite low AOD values (close to 0) before 6th Dec., both simulations with and without aerosols reasonably reproduced the temporal variation of downward SW at Beijing despite the slightly overestimation during the noon-time (Fig. 8a). However, the overestimated downward SW in NoAero turned to intensify extensively since 6th Dec. and sustained till 10th Dec., accompanied by the occurrence of the pollution with the high AOD value. Meanwhile, the downward SW was much lower in Aero than that in NoAero due to aerosol extinction, with resembled temporal variations and comparable magnitude at the peak time compared to the observations. Similarly, the variations of downward SW from Aero simulation were also closer to observations at Tianjin, Taiyuan and Jinan than those in NoAero (Figs. 8b-d). It was noted that the most significant improvement of simulated downward SW at Jinan appeared on 10th Dec. and was later than that at Beijing, which was consistent with the AOD's variations at Jinan. Moreover, the surface energy balance was also affected by the reduction of downward SW radiation reaching the ground due to the presence of aerosol particles. As shown in Figs. 8e–h, in corresponding to the changes in downward SW, the variations of net radiation at surface in Aero were also in better agreement with observation during the polluted period than in NoAero, particularly during daytime with the high AOD values.

To further quantify the influence of the aerosol-radiation interaction on the diurnal variation of surface radiation, next we compared the simulated averaged diurnal variation of downward SW and net radiation during the polluted episode (6th to 10th) with observation. Figure 9a showed that there existed a large overestimation of surface downward SW during the daytime in NoAero. Particularly, the overestimated downward SW tented to increase since morning (0800 LT) and peak at noon (1300 LT) with the maximum bias reaching 226.5 W m^{-2}, and the mean bias of ~149.4 W m^{-2} during daytime (averaged during 0800 to 1800 LT, Table 2). However, the overestimated SW radiation was remarkably reduced in Aero with the mean bias of 38.0 W m^{-2} during daytime. Similarly, the diurnal variation and magnitude of downward SW radiation at surface were also better captured at Tianjin, Taiyuan and Jinan in Aero (Figs. 9b–d), with the lower bias (70.9 W m^{-2}, 118.3 W m^{-2} and 97.7 W m^{-2}) than in NoAero (115.5 W m^{-2}, 155.0 W m^{-2} and 149.1 W m^{-2}) during daytime. Note the biases of SW radiation in Tianjin, Taiyuan and Jinan were not improved as much as in Beijing due to the lower AOD. Consistent with this finding, the reduction of downward SW was also reported in United States (Zhang et al., 2010) and Europe (Toll et al., 2016) with relatively lower decrease (10 W m^{-2} and 18 W m^{-2}); the relatively larger reductions (30-110 W m^{-2}) in northern China is possibly due to the higher aerosol load. Figures 9e–h presented the diurnal variations of net radiation, with positive (negative) net radiation during daytime (nighttime) in observation, and the NoAero tended to overestimate (underestimate) the net radiation at surface during daytime (nighttime), indicating that there existed surplus energy income and outcome in model than those in observation, inducing the larger magnitude of diurnal cycle of net radiation. By including the aerosol-radiation interaction in the model, the simulated diurnal variations of net radiation were markedly improved, particularly during daytime with the reduction of bias by 85.3%, 50.0%, 35.4%, and 44.1% at Beijing, Tianjin, Taiyuan and Jinan, respectively.

In response to the decrease of downward SW radiation and net radiation at the ground during daytime, the surface fluxes also changed in presence of aerosol extinction within the energy-balanced system. Figure 10 displayed the difference of surface sensible and latent heat flux between Aero and NoAero at 1300LT, when the influences of the aerosol on radiation reaching the peak. Comparing to the NoAero simulation, both the surface sensible and latent heat flux emitted by the surface were reduced in the Aero simulation, with the domain-average of 16.1 W m^{-2} (18.5%) and 6.8 W m^{-2} (13.4%) respectively. It was noted that the decrease of the surface latent heat flux was less pronounced than that of surface sensible heat flux, suggesting the impact of aerosol-radiation interaction on the humidity was less significant than that of temperature, which was also reported over United States (Fan et al., 2008) and western Europe (Péré et al., 2011).

3.2.2 Aerosol impacts on simulations of temperature, PBLH and wind fields

The changes in radiation and energy budget through the impacts of aerosol-radiation interaction would certainly induce the changes in PBL thermodynamics and dynamics, which would result in changes in the forecasts of meteorological fields. The impacts on the forecasts of 2-m temperature, PBLH and wind fields due to the aerosol-radiation interaction are discussed in the following subsection.

Figure 11 presented the diurnal variation of averaged bias of 2-m temperature during polluted period in NoAero (upper panel) and Aero (lower panel) compared with the in-situ observation during 1100 LT to 2300 LT. It was obvious that the temperature of NoAero was significantly overestimated for a wide range over northern China, particularly over the plain areas including south of Hebei, Henan and Shanxi provinces. The warm biases tended to intensify in the afternoon and reach ~3°C over south part of Hebei province (Figs. 11b–c). Accompanied by the warm biased over plain areas throughout the day, the mountain areas were dominated by the cold biases until 1700 LT, and turned to be warm biases afterwards, which were attributed by the frozen water in soil due to wet bias of soil moisture over mountain areas, inducing overestimated energy transport from atmosphere to soil during daytime. Compared to NoAero, the lower temperature in Aero due to the decreased surface solar radiation, caused by aerosol extinction led to the reduced warm bias in NCP region. However, the cold bias in Beijing area was slightly intensified, which may partly relevant with the overestimated $PM_{2.5}$ concentration in Beijing and can be improved by incorporating more accurate aerosol information in the future. It was noted that the cold biases over mountain areas associated with the model physics deficiency can not be corrected by aerosol-radiation effects, thus the correction of aerosol-radiation effect may get complex results and differ with regions due to the model pre-existing deficiencies.

To quantitatively evaluate the agreement of simulated 2-m temperature with observations, the mean bias and RMSE were employed, and their averaged diurnal variations during the polluted episode (6th to 10th, Dec.) averaged over NCP, denoted by the purple box in Fig. 1a, were displayed in Fig. 12. As shown in Fig. 12a, the warm bias in NoAero sustained during the entire 24-hr forecast, ranging from 0.3 °C to 0.9 °C. Compared to NoAero, the NCP area-averaged warm bias was remarkably reduced by ~0.40°C (~73.9%) due to aerosol-radiation interaction, with the maximum reaching ~0.54 °C (~95.0 %) at 1100 LT (Figs. 12a and c). Consistently with mean bias, the RMSE was also lower in Aero than NoAero, particularly during 1100 to 2000 LT during the daytime (Figs. 12b and d).

The aerosol-radiation interaction may also have profound impacts on atmospheric structure in addition to radiation and temperature (Rémy et al., 2015). PBLH is one of the key parameters to describe the structure of PBL and closely related to air pollution. It was indicated that the mean daytime PBLH over northern China were around 300–600m (Fig. 13a), and declined generally 40–200m (10%–40%) in Aero over the region with highest $PM_{2.5}$ concentration, particularly over Beijing, Tianjin and Hebei (Figs. 13b–c). As shown in dashed lines in Fig. 14, the NCP area-averaged PBLH at noon-time (1400 LT) was diminished dramatically by aerosol-radiation interaction during the pollution event over northern China, with the maximum decrease reaching -155.2m on 7th Dec. The reduction of PBLH could be the consequence of more stable atmosphere in Aero than NoAero, which was induced by the terrestrial cooling in the lower part of the planetary boundary layer and the solar heat due to the absorbing in the upper layers (solid lines in Fig. 14).

The near surface wind fields changes due to aerosol-radiation interaction were further investigated. Figure 15 shows the wind vector in NoAero (upper panel), Aero (middle panel) and their difference (lower panel). It can be seen from Fig. 15a-e that the northern China was dominated by the anticyclonic circulation, accompanied by the relatively weaker northeast wind over Beijing and Hebei areas. The comparisons of Aero and NoAero (Figs. 15 k-o) showed that the northeast wind was increased with the maximum reaching 1 m s^{-1} by aerosol-radiation interaction over Beijing and Hebei, where high particles concentration located (shadings in Figs. 15 f-j). Figures 15k-o also indicated the changes of west wind over the south part of the domain and southeast wind over the ocean areas, which tended to weaken the anticyclonic circulation and thus declined the wind speed there. The reduced wind speed due the inclusion of aerosol-radiation interaction was possible due to the thermal-wind adjustment in response to the more stable near-surface atmosphere, which was also addressed in previous work using WRF-Chem (Zhang et al., 2015).

The comparisons between simulated wind speeds against in-situ observation averaged during 6th to 10th Dec. were displayed in Fig. 16. In regard of NoAero, the simulated wind speed at 10m was overestimated over the nearly whole domain with the maximum bias up to 3 m s^{-1} except some mountain sites (upper and middle panels in Fig.16). It might be due to the omission of UCM model as the overestimation is more prominent in city clusters (especially in Beijing and southern Hebei) than other areas. Figures 16k-o showed the difference of absolute value of bias between Aero and NoAero and indicated the bias of simulated wind speed were decreased over south and northeast part of the domain during afternoon (Figs. 16k-m) by aerosol-radiation interaction, while were increased over Beijing and Hebei area particularly during nightfall (Fig. 16n) due to the intensified wind speed there. The NCP area-averaged bias and RMSE of wind speed at 10m were further shown in Figure 17. It was seen that the aerosol-radiation interaction helped to reduce the overestimation of wind speed at 10m up to 0.08 m s^{-1} (~7.8%), particular during daytime (Figs. 17a and c). Correspondingly, the RMSE of Aero was also lower than that of NoAero, indicating that the inclusion of aerosol-radiation interaction helped to improve the prediction of near surface wind speed on the domain-averaged scale.

Although the changes of wind speed are less straightforward than that of radiation, the aerosol-radiation interactions can also affect dynamic fields (vertical wind shear) through the changes of atmospheric thermal structure and the thermal wind relation when the interaction lasts long enough (Huang et al., 2019). Figure 18 displayed vertical profiles of wind speed at the stations of Beijing and Xingtai in simulation and verified with sounding observations. It was shown that the NoAero underestimated (overestimated) the low levels wind speed at 0800 LT (2000 LT) at both Beijing and Xingtai. However, the wind speed was increased (decreased) at 0800 LT (2000 LT) in Aero relative to NoAero, indicating the positive impacts on the simulation of atmospheric winds by aerosol-radiation interaction.

Since the forecast meteorological fields by WRF (RMPAS-ST) is routinely applied to WRF-Chem (RMAPS-Chem) as meteorological ICs in the air quality operational system at IUM, the changed meteorology due to aerosol-radiation interaction will further influence the forecast of pollution through meteorological ICs. In regard of further feedback of aerosol-radiation interactions to the transport and dissipation of the pollutants, their impacts on wind field at 850hPa were further discussed as it is strongly correlated with haze formation (Zhang et al., 2018; Zhai et al., 2019). Figures 19 a-e display that northern China was dominated by the anticyclone circulation at 850hPa, associated with the southwest (northwest) wind in the west (east) of the northern part of the domain. The difference of U (zonal, eastward is positive) winds between Aero and NoAero (middle panel in Fig. 16) showed that the U wind was intensified over west Hebei, accompanied by the quite small changes in Beijing area, indicating that the increased U wind was blocked by the mountains and could not transport the pollutants over Hebei and Beijing to the east (Figs. 19 f-h). On the other hand, the changes of V (meridional, northward is positive) show different patterns over north and south of the 38° N (lower panel in Fig. 19). In the south part, the increased northward wind due to aerosol-radiation interaction may help to transport pollutants from highly polluted areas to Hebei and Beijing. In the north of the domain, the negative (positive) changes of V wind indicated the reduced northward (southward) wind in west (east) of Hebei, which could suppress the diffusion of the pollutants. As a result, both U and V changes induced by the aerosol-radiation interaction will prevent pollutants from dispersing and may exacerbate the pollution in Heibei and Beijing, which confirms the more stable boundary layer due to aerosol-radiation interaction as discussed earlier.

4. Concluding remarks

To facilitate the future inclusion of aerosol-radiation interactions in the regional operational NWP system – RMAPS-ST (adapted from WRF) at IUM, CMA, the impacts of aerosol-radiation interactions on the forecast of surface radiation and meteorological parameters during a heavy pollution event (Dec. 6th -10th, 2015) over northern China were investigated. The aerosol information (550-nm AOD 2D field) were simulated by WRF-Chem and then offline-coupled into RRTMG radiation scheme of WRF to enable the aerosol-radiation feedback in the forecast. Two sets of

24-hour forecasts were performed at 00UTC from Dec. 2^{nd}-11^{th}, 2015. The only difference between the two sets of forecasts was whether the aerosol radiative feedback was activated (Aero, with WRF-Chem simulated hourly AOD fields as input fields) or not (NoAero, no aerosol included), while the other schemes remained the same.

The capability of WRF-chem to reproduce the polluted episode was confirmed first before the offline-coupling of AOD to WRF. The validation of simulated AOD and aerosol extinction coefficient against MODIS and CALIPSO confirmed that the model could reproduce both the spatial and vertical distribution of 550nm AOD. Further results indicated that the temporal variations of simulated AOD at 550nm was in consistent with AERONET and in-situ observation at IAP. In addition, the spatial distributions of $PM_{2.5}$ as well as their magnitude, particularly during the peak stage (8^{th} to 9^{th}) of the pollution event were reasonably captured by WRF-Chem, with the correlation coefficients of 0.85, 0.89, 0.76, 0.92 and 0.77 at Beijing, Shijiazhuang, Tianjin, Hebei and Henan, respectively.

Further, the impacts of aerosols-radiation interaction on the forecasts of surface radiation, energy budget, and meteorology parameters were evaluated against surface and sounding observations. The results showed that the decrease of downward SW radiation reaching surface induced by aerosol effects helped to reduce the overestimation of SW radiation during daytime. Moreover, the simulated surface radiation budget has also been improved, with the biases of net radiation at surface decreased by 85.3%, 50.0%, 35.4%, and 44.1% during daytime at Beijing, Tianjin, Taiyuan and Jinan respectively, accompanied by the reduction of sensible (16.1 W m^{-2}, 18.5%) and latent (6.8 W m^{-2}, 13.4%) heat fluxes emitted by the surface at noon-time.

The energy budget changed by aerosol extinction further cools 2-m temperature by ~0.40°C over NCP, reducing warm bias by ~73.9% and also leading to lower RMSE, particularly during daytime. Since aerosol cools the lower planetary boundary layer and meanwhile warms the high atmosphere, it induced the more stable stratification of the atmosphere and the declination of PBLH by 40–200m (10%–40%) over NCP. Associating with the changes of planetary boundary structure and more stable near-surface atmosphere, the aerosol-radiation interaction tended to weaken the anticyclonic circulation including the east wind over the south part of the domain and northwest wind over the ocean areas. Thus the bias of wind speed over south and northeast part of the domain were decreased particularly during the afternoon, while increased over Beijing and Hebei area. In regard of NCP-average, the overestimated 10m wind speed was improved during whole day with the maximum up to 0.08 m s^{-1} (~7.8%) at 1400LT. The comparison between simulated vertical profiles of atmospheric wind speed with soundings also indicated that Aero was in better agreement with observation and aerosol-radiation interaction helped to improve the prediction of dynamic fields such as atmospheric wind through the thermal wind relation by altering the atmospheric structure.

The impacts of aerosol-radiation interactions on wind field at 850hPa were further discussed. The results showed that aerosol-radiation interaction will prevent pollutants from dispersing and may exacerbate the pollution through changes of both U and V wind, which confirms the more stable boundary layer due to aerosol-radiation. These wind field changes may also influence the forecast of the transport and dissipation of the pollutants by WRF-Chem through changed meteorological ICs.

This study analyzed the impacts of aerosol-radiation interaction on radiation and meteorological forecast by using the offline-coupling of WRF and high-frequent updated AOD simulated by WRF-Chem, which is more computationally economic than the online simulation with the integration time for 96h forecast of about 40% of that for online simulation. This approach allows for a potential application to include aerosol-radiation interaction in our current operational NWP systems. The results revealed that aerosol-radiation interaction had profound influence on the improvement of predictive accuracy and the potential prospects for its application in regional NWP in northern China. Given that most of these analyses were based on a single case of pollution occurred during the wintertime of 2015, there is clearly a need for further research on more polluted cases to achieve more quantitative results before the operational application. As the simulated AOD was adopted in the present study, it should be noted that there exits a discrepancy between simulated AOD and observation in both spatial distribution and temporal variation, which may influence the impacts of aerosol-radiation interaction. Meanwhile, surface energy budget and atmospheric dynamics are also influenced by aerosol-cloud interaction, which are related to cloud microphysical processes and are not discussed in this study.

Data availability Data are available upon request from the first authors Yang Yang (yyang@ium.cn) and corresponding authors Xiujuan Zhao (xjzhao@ium.cn) and Dan Chen (dchen@ium.cn).

Author contribution Yang Yang, Min Chen, Xiujuan Zhao and Dan Chen designed the experiments, Yang Yang and Xiujuan Zhao performed the simulations and carried them out. Yang Yang and Dan Chen prepared the manuscript with contributions from all co-authors.

Competing interests The authors declare that they have no conflict of interest.

Acknowledgments This work was jointly supported by the National Key R&D Program of China (grant nos. 2017YFC1501406 and 2018YFF0300102), Natural Science Foundation of Beijing Municipality (8161004), the National Natural Science Foundation of China (grant nos. 41705076, 41705087 and 41705135), Beijing Major Science and Technology Project (Z181100005418014) and Beijing Natural Science Foundation (grant no. 8204074).

Reference

Ackerman, A. S., Toon, O. B., Stevens, D. E., Heymsfield, A. J., Ramanathan, V., and Welton, E. J.: Reduction of tropical cloudiness by soot, Science, 288, 1042–1047, https://doi.org/10.1126/science.288.5468.1042, 2000.

Baklanov, A., Schlünzen, K., Suppan, P., Baldasano, J., Brunner, D., Aksoyoglu, S., Carmichael, G., Douros, J., Flemming, J., Forkel, R., Galmarini, S., Gauss, M., Grell, G., Hirtl, M., Joffre, S., Jorba, O., Kaas, E., Kaasik, M., Kallos, G., Kong, X., Korsholm, U., Kurganskiy, A., Kushta, J., Lohmann, U., Mahura, A., Manders-Groot, A., Maurizi, A., Moussiopoulos, N., Rao, S. T., Savage, N., Seigneur, C., Sokhi, R. S., Solazzo, E., Solomos, S., Sørensen, B., Tsegas, G., Vignati, E., Vogel, B., and Zhang, Y.: Online coupled regional meteorology chemistry models in Europe: current status and prospects, Atmos. Chem. Phys., 14, 317–398, https://doi.org/10.5194/acp-14-317-2014, 2014.

Chan, C. K. and Yao, X.: Air pollution in mega cities in China, Atmos. Environ., 42, 1–42, https://doi.org/10.1016/j.atmosenv.2007.09.003, 2008.

Chen, D., Liu, Z., Davis, C., and Gu, Y.: Dust radiative effects on atmospheric thermodynamics and tropical cyclogenesis over the Atlantic Ocean using WRF-Chem coupled with an AOD data assimilation system, Atmos. Chem. Phys., 17, 7917–7939, https://doi.org/10.5194/acp-17-7917-2017, 2017.

Chen, F. and Dudhia, J.: Coupling an advanced land surface-hydrology model with the Penn State-NCAR MM5 modeling system. Part I: Model implementation and sensitivity, Mon. Wea. Rev., 129, 569–585, doi: 10.1175/1520-0493(2001)129<0569:CAALSH>2.0.CO;2, 2001.

Cheng, X., Sun, Z., Li, D., Xu, X., Jia, M., and Cheng, S.: Short-term aerosol radiative effects and their regional difference during heavy haze episodes in January 2013 in China, Atmos. Environ., 165, 248–263, http://dx.doi.org/10.1016/j.atmosenv.2017.06.040, 2017.

Cheng, Y. F., Eichler, H., Wiedensohler, A., Heintzenberg, J., Zhang, Y. H., Hu, M., Herrmann, H., Zeng, L.M., Liu, S., Gnauk, T., Brüggemann, E., and He, L.Y., Mixing state of elemental carbon and non-light-absorbing aerosol components derived from in situ particle optical properties at Xinken in Pearl River Delta of China, J. Geophys. Res.-Atmos.,111, D20204, doi: 10.1029/2005JD006929, 2006.

Chou, M. D. and Suarez, M. J.: A solar radiation parameterization for atmospheric studies, Tech. Rep. NASA/TM-1999-104606, 15, Technical Report Series on Global Modeling and Data Assimilation NASA, 1999.

Ek, M. B., Mitchell, K. E., Lin, Y., Rogers, E., Grunmann, P., Koren, V., Gayno, G., and Tarpley, J.D.: Implementation of Noah land surface model advances in the National Centers for Environmental Prediction operational mesoscale Eta model, J. Geophys. Res.-Atmos, 108, 8851, doi:10.1029/2002JD003296, 2003.

Elser, M., Huang, R.-J., Wolf, R., Slowik, J. G., Wang, Q., Canonaco, F., Li, G., Bozzetti, C., Daellenbach, K. R., Huang, Y., Zhang, R., Li, Z., Cao, J., Baltensperger, U., El-Haddad, I., and Prévôt, A. S. H.: New insights into $PM_{2.5}$ chemical composition and sources in two major cities in China during extreme haze events using aerosol mass spectrometry, Atmos. Chem. Phys., 16, 3207–3225, https://doi.org/10.5194/acp-16-3207-2016, 2016.

Fan, J., Zhang, R., Tao, W. K., and Mhor, K. I.: Effects of aerosol optical properties on deep convective clouds and radiative forcing, J. Geophys. Res., 113, D08209, doi:10.1029/2007JD009257, 2008.

Ghan, S. J., Liu, X., Easter, R. C., Zaveri, R., Rasch, P. J., Yoon, J.-H., Eaton, B.: Toward a Minimal Representation of Aerosols in Climate Models: Comparative Decomposition of Aerosol Direct, Semidirect, and Indirect Radiative Forcing, J. Clim., 2012, 25, 6461-6476, doi: 10.1175/JCLI-D-11-00650.1, 2012.

Grell, G. A. and Baklanov, A.: Integrated modelling for forecasting weather and air quality: a call for fully coupled approaches, Atmos. Environ., 45, 6845–6851, https://doi.org/10.1016/j.atmosenv.2011.01.017, 2011.

Grell, G. A. and Dévényi, D.: A generalized approach to parameterizing convection combining ensemble and data assimilation techniques, Geophys. Res. Lett., 29, 1693, doi: 10.1029/2002GL015311, 2002.

Grell, G., Freitas, S. R., Stuefer, M., and Fast, J.: Inclusion of biomass burning in WRF-Chem: impact of wildfires on weather forecasts, Atmos. Chem. Phys., 11, 5289-5303, https://doi.org/10.5194/acp-11-5289-2011, 2011.

Guo, J., Deng, M., Lee, S. S., Wang, F., Li, Z., Zhai, P., Liu, H., Lv, W., Yao, W., and

Li, X.,: Delaying precipitation and lightning by air pollution over the pearl river delta. Part I: observational analyses, J. Geophys. Res.-Atmos, 121, 6472–6488, doi:10.1002/2015JD023257, 2016.

Hansen, J., Sato, M., and Ruedy, R.: Radiative forcing and climate response, J. Geophys. Res.-Atmos, 102, 6831–6864, https://doi.org/10.1029/96JD03436, 1997.

Hong, S.-Y., Noh, Y., and Dudhia, J.: A new vertical diffusion package with an explicit treatment of entrainment processes, Mon. Weather Rev., 134, 2318–2341, doi:10.1175/Mwr3199.1, 2006.

Huang, C.-C., Chen, S.-H., Lin, Y.-C., Earl, K., Matsui, T., Lee, H.-H., Tsai, I-C., Chen, J.-P., and Cheng, C.-T.: Impacts of Dust–Radiation versus Dust–Cloud Interactions on the Development of a Modeled Mesoscale Convective System over North Africa, Mon. Weather Rev., 47, 3301-3326. https://doi.org/10.1175/MWR-D-18-0459.1, 2019.

Huang, X., Ding, A., Liu, L., Liu, Q., Ding, K., Niu, X., Nie, W., Xu, Z., Chi, X., Wang, M., Sun, J., Guo, W., and Fu, C.: Effects of aerosol–radiation interaction on precipitation during biomass-burning season in East China, Atmos. Chem. Phys., 16, 10063 – 10082, https://doi.org/10.5194/acp-16-10063-2016, 2016.

Iacono, M. J., Delamere, J. S., Mlawer, E. J., Shephard, M. W., Clough, S. A., Collins, W. D.: Radiative forcing by long-lived greenhouse gases: Calculations with the AER radiative transfer models, J. Geophys. Res.-Atmos,113, D13, doi:

10.1029/2008JD009944, 2008.

Kain, J. S.: The Kain-Fritsch convective parameterization: An update, J. Appl. Meteorol., 43, 170–181, 2004.

Kaufman, Y. J., Tanre, D., and Boucher, O.: A satellite view of aerosols in the climate system, Nature, 419, 215-223, http://dx.doi.org/10.1038/nature01091, 2002.

Liao, H., Chen, W. T., and Seinfeld, J. H.: Role of climate change in global predictions of future tropospheric ozone and aerosols, J. Geophys. Res., 111, D12304, doi:10.1029/2005JD006852, 2006.

Liao, L., Lou, S. J., Fu, Y., Chang, W. J., and Liao, H.: Radiative forcing of aerosols andits impact on surface air temperature on the synoptic scale in eastern China, Chinese J. Atmos. Sci. (in Chinese), 39, 68–82.,doi: doi: 10.3878/j.issn.1006-9895.1402.13302, 2015.

Liu, X., Zhang, Y., Cheng, Y., Hu, M., and Han, T.: Aerosol hygroscopicity and its impact on atmospheric visibility and radiative forcing in Guangzhou during the 2006 PRIDE-PRD campaign, Atmos. Environ. 60, 59–67, https://doi.org/10.1016/j.atmosenv.2012.06.016, 2012.

Mlawer, E. J., Taubman, S. J., Brown, P. D., Iacono, M. J. and Clough, S. A.: Radiative transfer for inhomogeneous atmospheres: RRTM, a validated correlated-k model for the longwave, J. Geophys. Res., 102, doi:10.1029/97JD00237. 16663-16682, 1997.

Mulcahy, J. P., Walters, D. N., Bellouin, N., and Milton, S. F.: Impacts of increasing the aerosol complexity in the Met Office global numerical weather prediction model, Atmos. Chem. Phys., 14, 4749–4778, https://doi.org/10.5194/acp-14-4749-2014, 2014.

Oreopoulos, L., Mlawer, E., Delamere, J., Shippert, T., Cole, J., Fomin, B., Iacono, M., Jin, Z., Li, J., Manners, J., Räisä-nen, P., Rose, F., Zhang, Y., Wilson, M. J., and Rossow, W. B.: The Continual Intercomparison of Radiation Codes: Results from Phase I, J. Geophys. Res.-Atmos., 117, D06118, https://doi.org/10.1029/2011JD016821, 2012.

Péré, J. C., Mallet, M., Pont, V., and Bessagnet B.: Impact of aerosol direct radiative forcing on the radiative budget, surface heat fluxes, and atmospheric dynamics during the heat wave of summer 2003 over western Europe: A modeling study, J. Geophys. Res., 116, D23119, https://doi.org/10.1029/2011JD016240, 2011.

Pleim. J. E.: A Combined local and nonlocal closure model for the atmospheric boundary layer. Part I: Model description and testing, J. Appl. Meteorol. Climat., 46, 1383–1395, doi: 10.1175/JAM2539.1, 2007.

Quan, J., Tie, X., Zhang, Q., Liu, Q., Li, X., Gao, Y., and Zhao D.: (2014). Characteristics of heavy aerosol pollution during the 2012–2013 winter in beijing, China, Atmos. Environ., 88, 83-89, https://doi.org/10.1016/j.atmosenv.2014.01.058, 2014.

Ramanathan, V., Crutzen, P. J., Kiehl, J. T., and Rosenfeld, D.: Aerosols, Climate and the Hydrological Cycle, Science, 294, 2119–2124, 2001.

Rémy, S., Benedetti, A., Bozzo, A., Haiden, T., Jones, L., Razinger, M., Flemming, J., Engelen, R. J., Peuch, V. H., and Thepaut, J. N.: Feedbacks of dust and boundary layer meteorology during a dust storm in the eastern Mediterranean, Atmos. Chem. Phys., 15, 12909–12933, https://doi.org/10.5194/acp-15-12909-2015, 2015.

Rodwell, M. J. and Jung T.: Understanding the local and global impacts of model physics changes: an aerosol example, Q. J. Roy. Meteor. Soc., 134, 1479-1497, https://doi.org/10.1002/qj.298, 2008.

Rogers, R. E., Deng, A. J., Stauffer, D. R., Gaudet, B. J., Jia, Y. Q., Soong, S. T., and Tanrikulu, S.: Application of the Weather Research and Forecasting Model for Air Quality Modeling in the San Francisco Bay Area, J. Appl. Meteor. Clim., 52, 1953–1973, doi: 10.1175/JAMC-D-12-0280.1, 2013.

Ruiz-Arias, J. A., Dudhia, J., and Gueymard, C. A.: A simple parameterization of the short-wave aerosol optical properties for surface direct and diffuse irradiances assessment in a numerical weather model, Geosci. Model Dev., 7, 1159–1174, doi:10.5194/gmd-7-1159-2014, 2014.

Sekiguchi, A., Shimadera, H., and Kondo, A.: 2018, Impact of Aerosol Direct Effect on Wintertime $PM_{2.5}$ Simulated by an Online Coupled Meteorology-Air Quality Model over East Asia, Aerosol and Air Quality Research, 18: 1068–1079, doi: 10.4209/aaqr.2016.06.0282, 2018.

Thompson, G., Field, P. R., Rasmussen, R. M., and Hall, W. D.: Explicit forecasts of winter precipitation using an improved bulk microphysics scheme. Part II: Implementation of a new snow parameterization, Mon. Weather Rev., 136, 5095–5115, https://doi.org/10.1175/2008MWR2387.1, 2008.

Toll, V., Gleeson, E., Nielsen, K.P., Männik, A., Mašek, J., Rontu, L., and Post, P.: Impacts of the direct radiative effect of aerosols in numerical weather prediction over Europe using the ALADIN-HIRLAM NWP system, Atmos. Res., 172-173, 163-173, https://doi.org/10.1016/j.atmosres.2016.01.003, 2016.

Toll, V., Reis. K., Ots, R., Kaasik, M., Männik, A., Prank, M., Sofiev, M.: SILAM and MACC reanalysis aerosol data used for simulating the aerosol direct radiative effect with the NWP model HARMONIE for summer 2010 wildfire case in Russia, Atmos. Environ., 121, 75-85, https://doi.org/10.1016/j.atmosenv.2015.06.007, 2015.

Wang, H., Shi, G. Y., Zhang, X. Y., Gong, S. L., Tan, S. C., Chen, B., Che, H. Z., and Li, T.: Mesoscale modelling study of the interactions between aerosols and PBL meteorology during a haze episode in China Jing–Jin–Ji and its near surrounding region – Part 2: Aerosols' radiative feedback effects, Atmos. Chem. Phys., 15, 3277-3287, https://doi.org/10.5194/acp-15-3277-2015, 2015b.

Wang, H., Xue, M., Zhang, X. Y., Liu, H. L., Zhou, C. H., Tan, S. C., Che, H. Z., Chen, B., and Li, T.: Mesoscale modeling study of the interactions between aerosols and PBL meteorology during a haze episode in Jing–Jin–Ji (China) and its nearby surrounding region – Part 1: Aerosol distributions and meteorological features, Atmos. Chem. Phys., 15, 3257–3275, https://doi.org/10.5194/acp-15-3257-2015, 2015a.

Wang, J., Wang, S., Jiang, J., Ding, A., Zheng, M., Zhao, B., Wong, D. C., Zhou, W., Zheng, G., Wang, L., Pleim, J. E. and Hao, J.: Impact of aerosol–meteorology interactions on fine particle pollution during China's severe haze episode in January 2013, Environ. Res. Lett., 9, 094002, doi:10.1088/1748-9326/9/9/094002, 2014.

Wang, X, He, X., Miao, S., Dou, Y.: Numerical simulation of the influence of aerosol radiation effect on urban boundary layer, Sci. China Earth Sci., 61, 1844–1858, https://doi.org/10.1007/s11430-018-9260-0, 2018.

Yang, X., Zhao, C., Zhou, L., Wang, Y., Liu, X.: Distinct impact of different types of aerosols on surface solar radiation in China, J. Geophys. Res.-Atmos., 121, 6459-6471, doi: 10.1002/2016JD024938, 2017b.

Yang, Y. and Ren, R. C.: On the contrasting decadal changes of diurnal surface temperature range between the Tibetan Plateau and southeastern China during the 1980s–2000s, Adv. Atmos. Sci., 34, 181–198, doi: 10.1007/s00376-016-6077-z, 2017a.

Yu, H., Kaufman, Y. J., Chin, M., Feingold, G., Remer, L. A., Anderson, T. L., Balkanski, Y., Bellouin, N., Boucher, O., Christopher, S., DeCola, P., Kahn, R., Koch, D., Loeb, N., Reddy, M. S., Schulz, M., Takemura, T., and Zhou, M.: A review of measurement-based assessments of the aerosol direct radiative effect and forcing, Atmos. Chem. Phys., 6, 613-666, https://doi.org/10.5194/acp-6-613-2006, 2006.

Zaveri, R. A. and Peters, L. K.: A new lumped structure photochemical mechanism for large-scale applications, J. Geophys. Res., 104, 30387–30415, https://doi.org/10.1029/1999JD900876,1999.

Zhai, S., Jacob, D. J., Wang, X., Shen, L., Li, K., Zhang, Y., Gui, K., Zhao, T., and Liao, H.: Fine particulate matter ($PM_{2.5}$) trends in China, 2013–2018: separating contributions from anthropogenic emissions and meteorology, Atmos. Chem. Phys., 19, 11031-11041, https://doi.org/10.5194/acp-19-11031-2019, 2019.

Zhang, B., Wang, Y., and Hao, J.: Simulating aerosol–radiation–cloud feedbacks on meteorology and air quality over eastern China under severe haze conditionsin winter, Atmos. Chem. Phys., 15, 2387-2404, https://doi.org/10.5194/acp-15-2387-2015, 2015.

Zhang, Q., Ma, Q., Zhao, B., Liu, X., Wang, Y., Jia, B., and Zhang, X.: Winter haze over North China Plain from 2009 to 2016: Influence of emission and meteorology, Environ. Pollut., 242, 1308–1318. doi:10.1016/j.envpol.2018.08.019, 2018.

Zhang, Q., Quan, J., Tie, X., Li, X., Liu, Q., Gao, Y., and Zhao, D. L.: Effects of meteorology and secondary particle formation on visibility during heavy haze events in Beijing, China, Sci. Total Environ., 502, 578–584, https://doi.org/10.1016/j.scitotenv.2014.09.079, 2015.

Zhang, Y., Wen, X.-Y., and Jang, C.-J.: Simulating chemistry-aerosol-cloud-radiation-climate feedbacks over the continental U.S. using the online-coupled Weather Research Forecasting Model with chemistry (WRF/Chem), Atmos. Environ. 44, 3568–3582, https://doi.org/10.1016/j.atmosenv.2010.05.056, 2010.

Zhang, Y.-Z, Miao, S.-G., Dai, Y.-J., Liu, Y.-H., Numerical simulation of characteristics of summer clear day boundary layer in Beijing and the impact of urban underlying surface on sea breeze (in Chinese), Chin J. Geophys, 56, 2558–2573, 2013.

Zhao, X., Li, Z., Xu, J.: Modification and performance tests of visibility parameterizations for haze days, Environ. Sci., 40, 1688-1696 (in Chinese), 2019.

Zheng, Y., Che, H., Xia, X., Wang, Y., Wang, H., Wu, Y., Tao, J., Zhao, H., An, J., Li, L., Gui, K., Sun, T., Li, X., Sheng, Z., Liu, C., Yang, X., Liang, Y., Zhang, L., Liu, C., Kuang, X., Luo, S., You, Y., and Zhang, X.: Five-year observation of aerosol optical properties and its radiative effects to planetary boundary layer during air pollution episodes in North China: Intercomparison of a plain site and a mountainous site in Beijing, Sci. Total Environ., 674, 140–158. https://doi.org/10.1016/j.scitotenv.2019.03.418, 2019.

Table 1. The variables, sources, numbers of sites in the domain/NCP and the frequency of chemical and meteorological observations.

Variables	Source of observation	Numbers of sites over the domain/NCP	Frequency	locations
AOD	AERONET	3/3	hourly	black dots in Fig. 1b
AOD	IAP station	1/1	hourly	blue dot in Fig. 1b
AOD	MODIS	/	daily	Fig. 2f-j and Fig. 2p-t
aerosol extinction coefficient	CALIPSO	/	daily	black paths in Fig.3a-d
$PM_{2.5}$	China National Environmental Monitoring Centre	813/332	hourly	dots in Fig. 5a
radiation	China Meteorological Administration	4/4	hourly	triangles in Fig. 1a
radiation	IAP station	1/1	hourly	triangles in Fig. 1a
2-m temperature	China Meteorological Administration	1157/534	hourly	dots in Fig. 11a
wind at 10m	China Meteorological Administration	1157/534	hourly	dots in Fig. 11a
atmospheric wind	China Meteorological Administration	2/2	0800LT, 2000LT	circles in Fig. 1a

Table 2. Mean bias of downward SW radiation at surface (W m^{-2}) and Net radiation at surface (W m^{-2}) from NoAero and Aero relative to observation during daytime (averaged 0800 to 1800 LT) and nighttime (averaged 1900 to 0700 LT), averaged from 6th to 11th Dec. 2015 at Beijing, Tianjin, Taiyuan and Jinan respectively.

Station	SW radiation		Net radiation			
	Daytime		Daytime		Nighttime	
	NoAero	Aero	NoAero	Aero	NoAero	Aero
Beijing	149.4	38.0	102.2	15.0	-33.6	-33.2
Tianjin	115.5	70.9	72.2	36.4	-27.1	-26.4
Taiyuan	155.0	118.3	66.9	43.2	-33.6	-33.3
Jinan	149.1	97.7	81.2	45.3	-30.3	-29.3

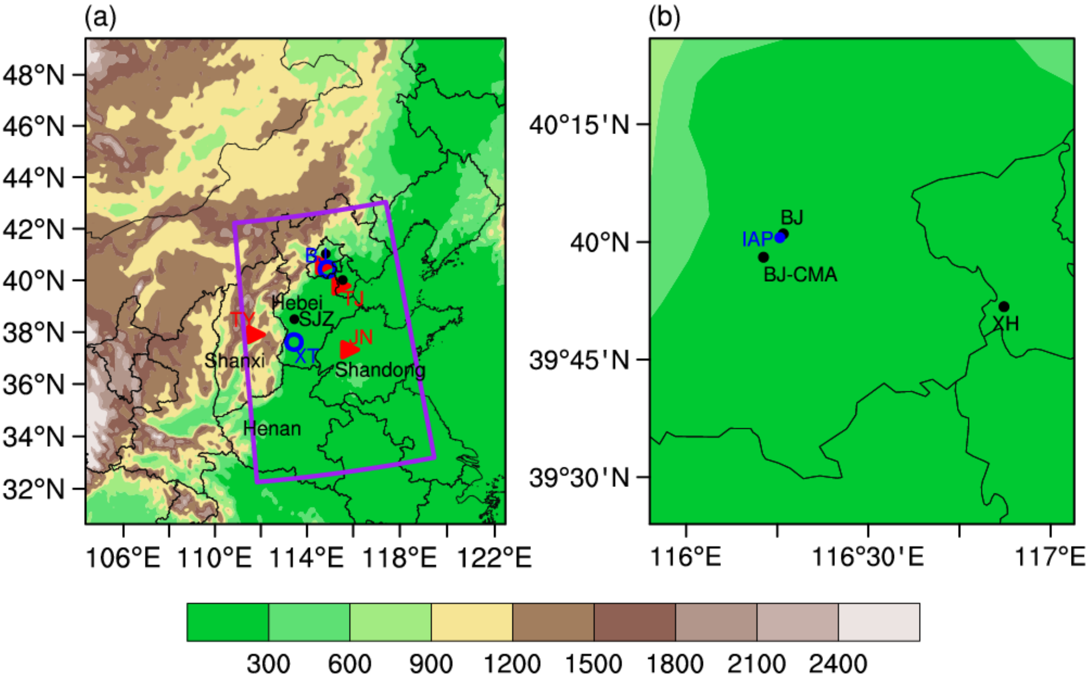

Figure 1. (a) The model domain and the terrain height (shadings, m). Purple box denotes the NCP, triangles are the observational sites of radiation (BJ: Beijing, TJ: Tianjin, TY: Taiyuan and JN: Jinan), circles are sites of sounding observation (BJ: Beijing and XT: Xingtai), dots denote the major cities for validation of $PM_{2.5}$ (BJ: Beijing, SJZ: Shijiazhuang and TJ: Tianjin). Names of provinces are also added (Hebei, Shanxi, Shandong and Henan). (b) The observational sites of AOD, including AERONET sites (black dots, BJ: Beijing, BJ-CMA: Beijing-CMA and XH: Xianghe) and IAP in-situ (blue dot) site.

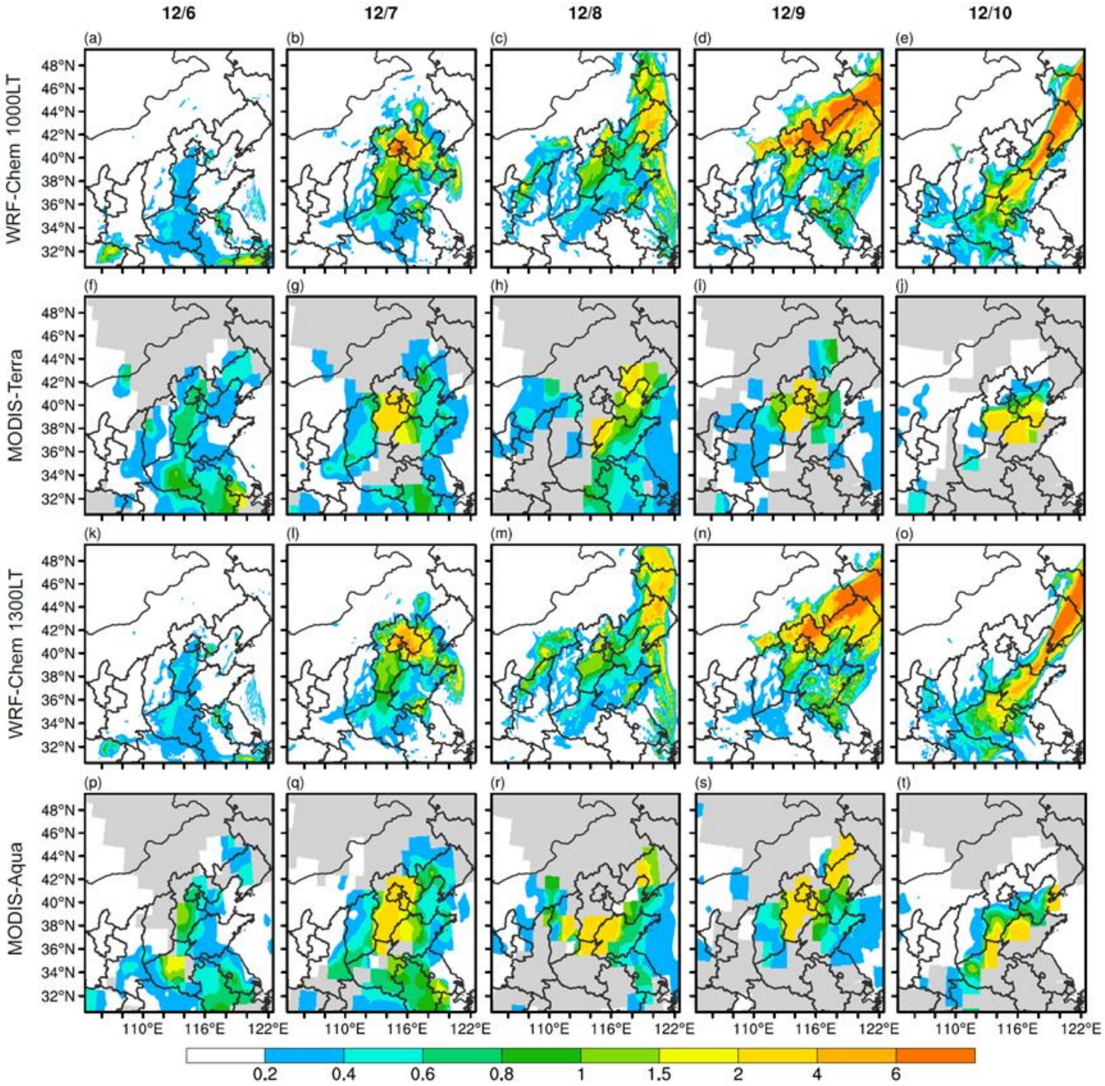

Figure 2. The WRF-Chem simulated and MODIS observed spatial distribution of AOD on 6th-10th December (from left to right). The first (a-e) and third rows (k-o) are WRF-Chem simulations at 1000LT and 1300LT (MODIS path times) respectively. The second (f-j) and fourth (p-t) rows are MODIS Terra and Aqua observations, respectively. Gray areas in (f-j) and (p-t) denote the missing values.

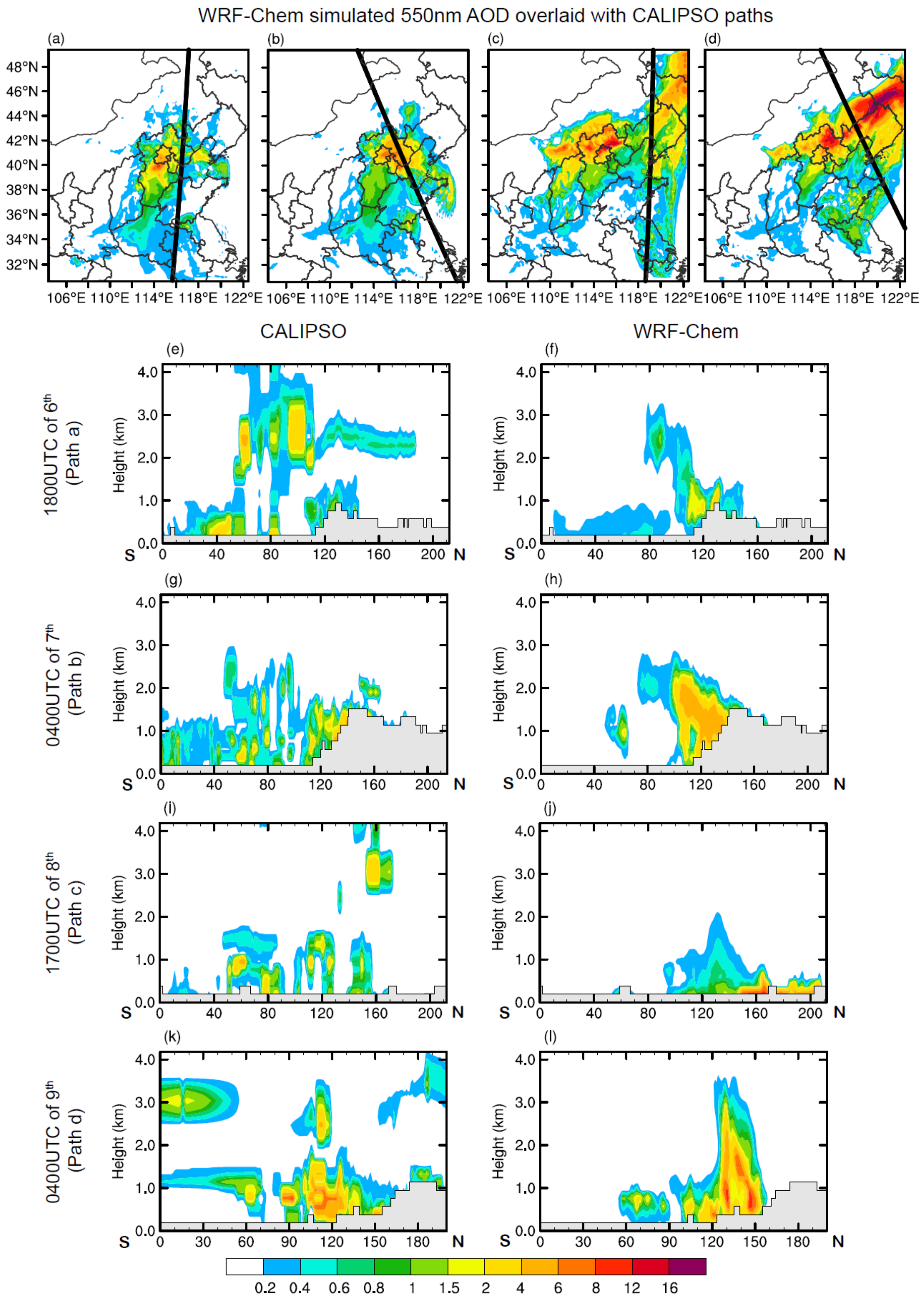

Figure 3. The WRF-Chem simulated 550nm AOD (shadings) on (a)1800UTC of 6th, (b) 0400UTC of 7th, (c)1700UTC of 8th, (d) 0400UTC of 9th December overlaid with CALIPSO paths (black thick solid). (e-l) denote the corresponding vertical

distributions of aerosol extinction coefficient at 550nm from (e, g, i, k) CALIPSO and (f, h, j, l) model simulations. Gray areas in (e-l) denote the terrain.

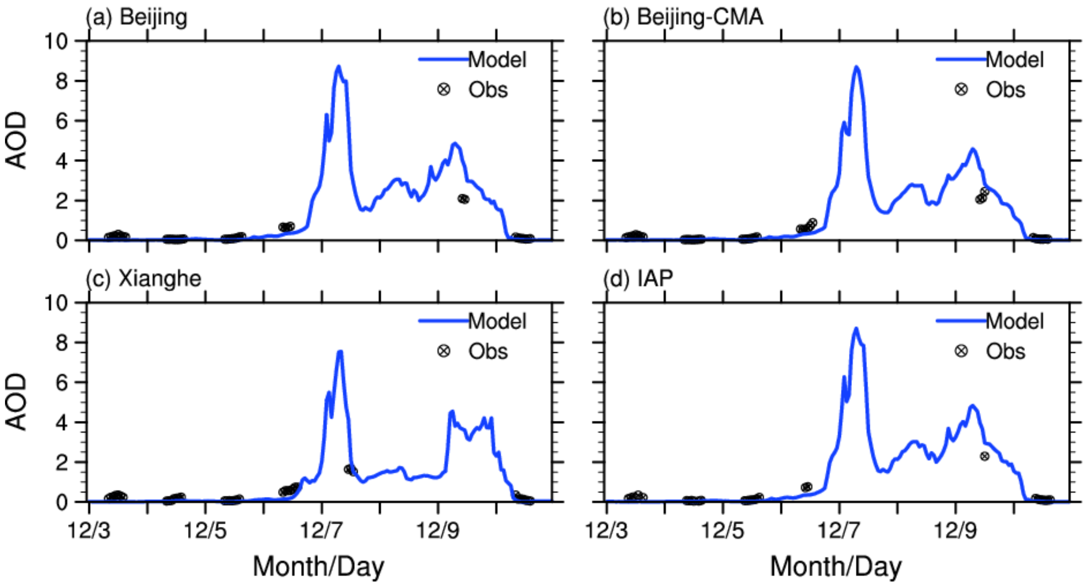

Figure 4. Temporal variation of observed (black dots) and simulated (blue) AOD at 550nm during 3rd-10th Dec. (LT) at (a) Beijing, (b) Beijing-CMA, (c) Xianghe and (d) IAP, AOD observations are from (a-c) AERONET and (d) IAP in-situ site.

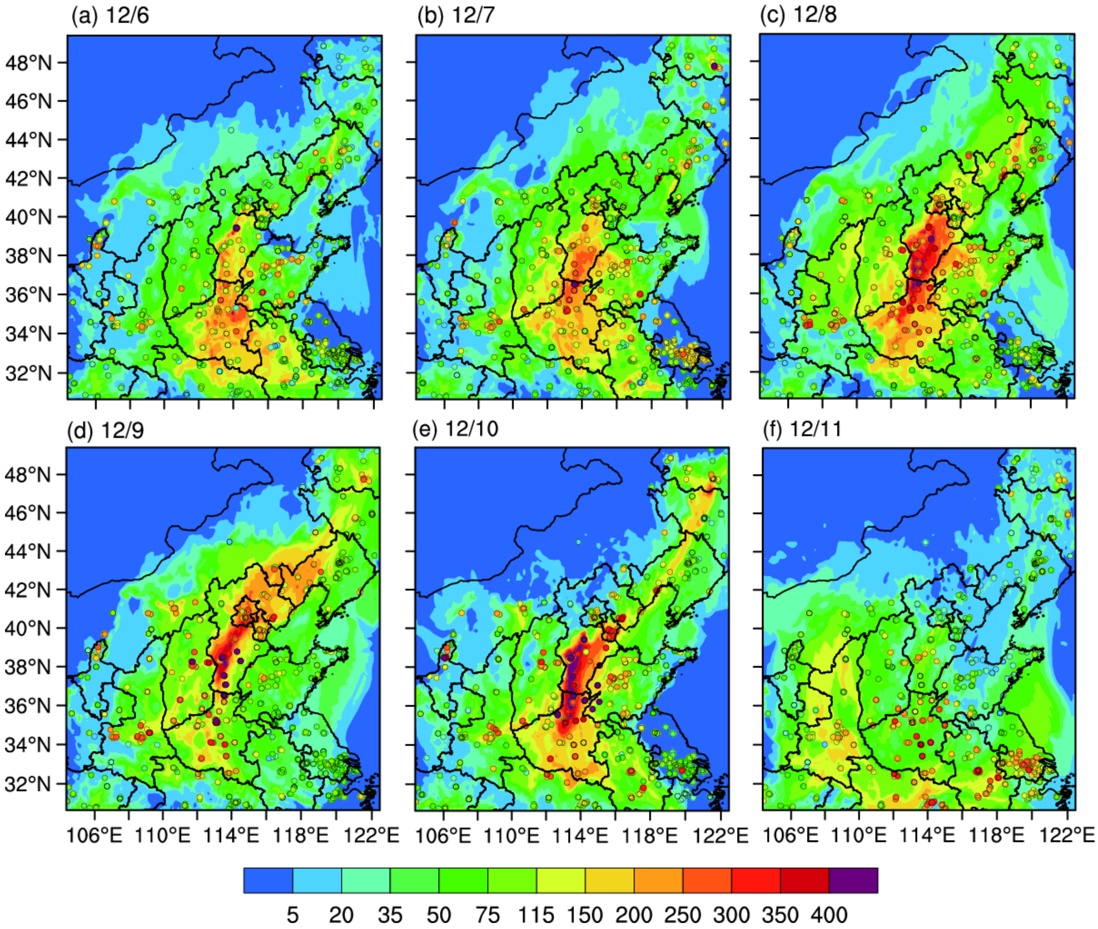

Figure 5. Observed (colored dots) and WRF-Chem simulated (shadings) spatial distribution of $PM_{2.5}$ concentrations (μg m^{-3}) on 0800LT of (a) 6th, (b) 7th, (c) 8th, (d) 9th, (e) 10th and (f) 11th Dec. respectively.

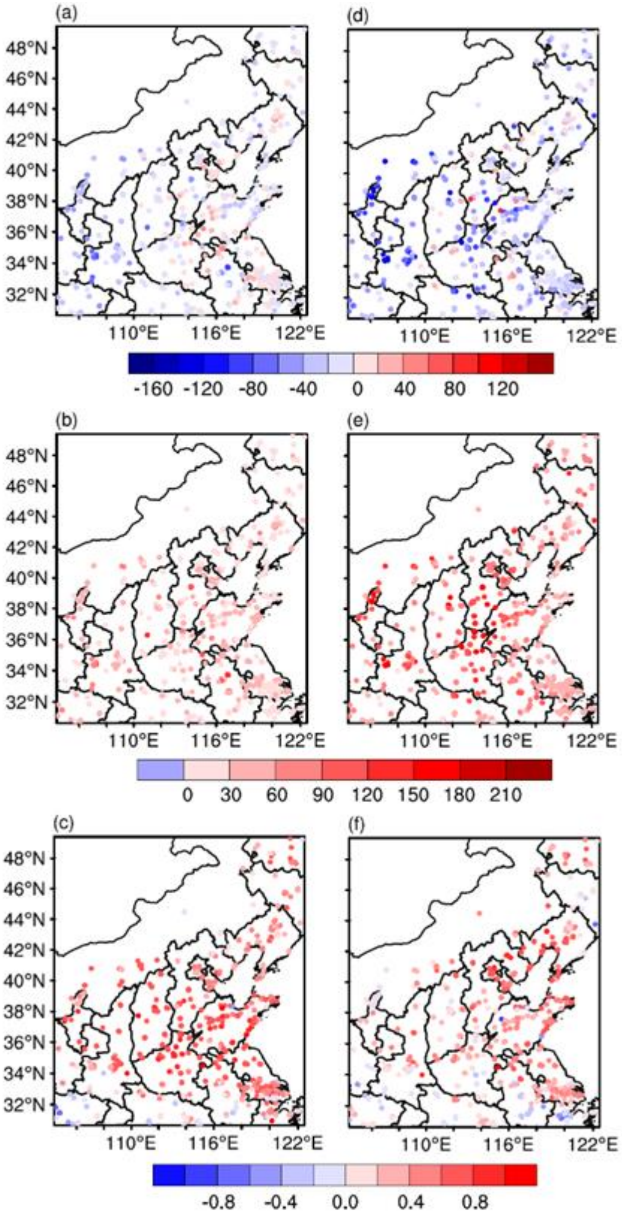

Figure 6. The (a, d) bias (μg m^{-3}), (b, e) RMSE (μg m−3), and (c, f) correlation coefficient (1) averaged (a-c) during clean period (3th to 5th Dec.) and (d-f) the polluted period (6th to 10th December).

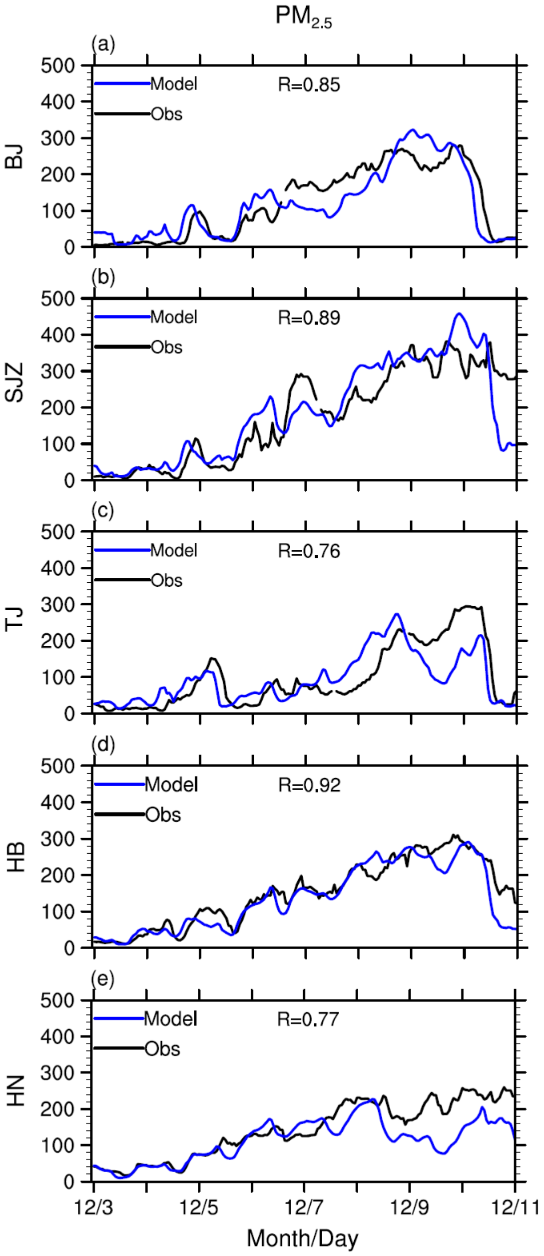

Figure 7. Observed (black) and WRF-Chem simulated (blue) temporal variation of $PM_{2.5}$ (μg m^{-3}) at three major cities (a) Beijing (BJ), (b) Shijiazhuang (SJZ) (c)Tianjin (TJ) and two provinces (d) Hebei (HB) and (e) Henan (HN).

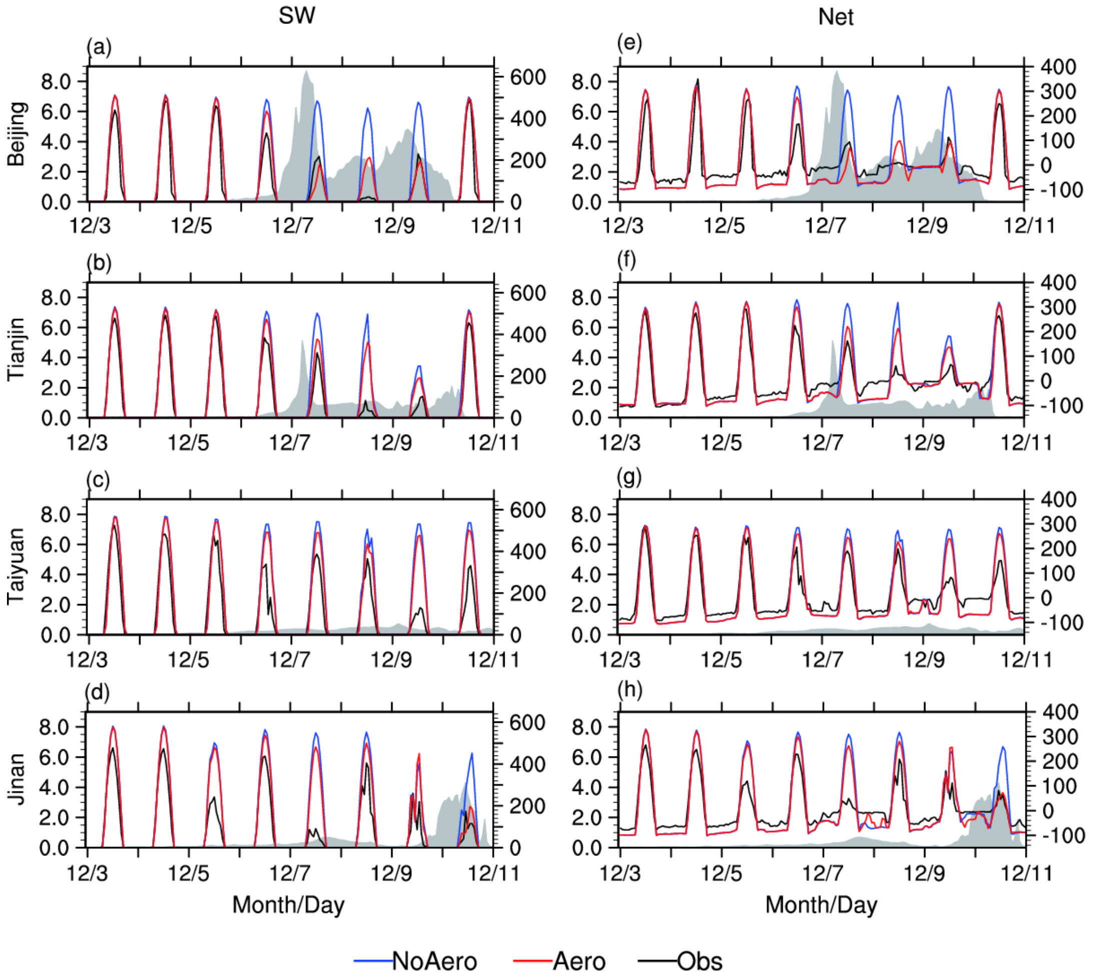

Figure 8. (a–d) observed (black) and WRF simulated (NoAero: blue, Aero: red) temporal variation of downward shortwave radaition at surface (W m^{-2}, right axis) at (a) Beijing, (b) Tianjin, (c) Taiyuan and (d) Jinan, respectively. The grey areas indicate the simulated AOD (left axis) by WRF-Chem. (e–h) are same with (a–d), but for net radaition at surface (W m^{-2}).

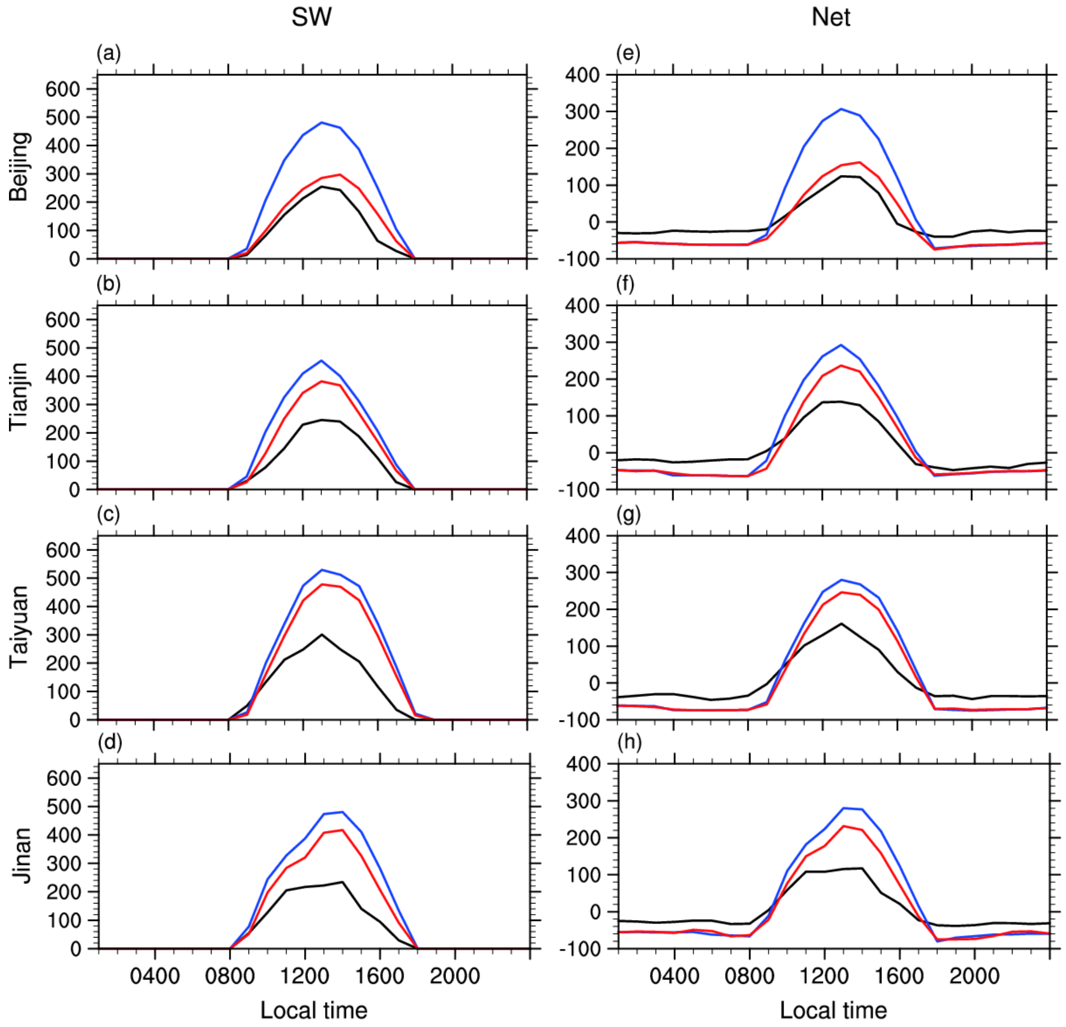

871

872 Figure 9. (a–d) observed (black) and simulated (NoAero: blue, Aero: red) diurnal cycles of downward shortwave radaition at surface (W m^{-2}) averaged from 6th to 10th Dec. 2015 at (a) Beijing, (b) Tianjin, (c) Taiyuan and (d) Jinan, respectively. (e–h) are same with (a–d), but for net radaition at surface (W m^{-2}).

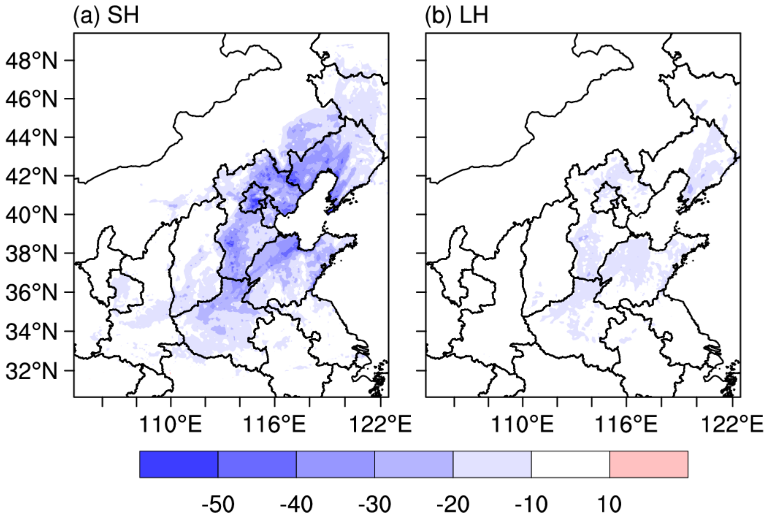

Figure 10. The differences (Aero minus NoAero) of (a) surface sensible heat flux and (b) surface latent heat flux (W m^{-2}, upward is positive) at 1300LT averaged from 6th to 10th Dec. 2015.

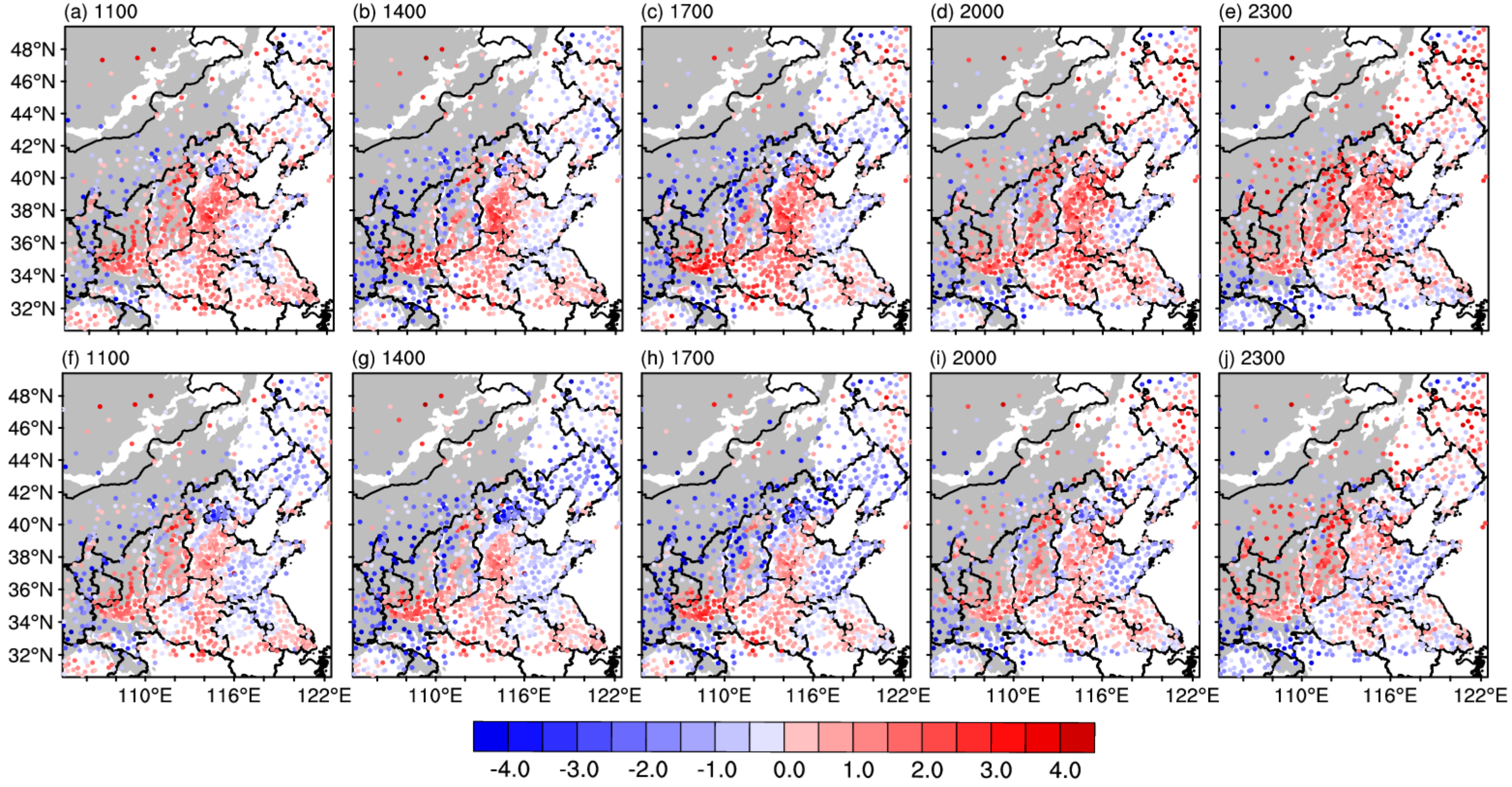

Figure 11. The bias of 2-m temperature (°C) at (a) 1100, (b) 1400, (c) 1700, (d) 2000 and (e) 2300 LT in NoAero averaged from 6th to 10th Dec. 2015, (f–j) are same with (a–e), but for Aero. The grey areas denote the areas of terrain height above 1000m.

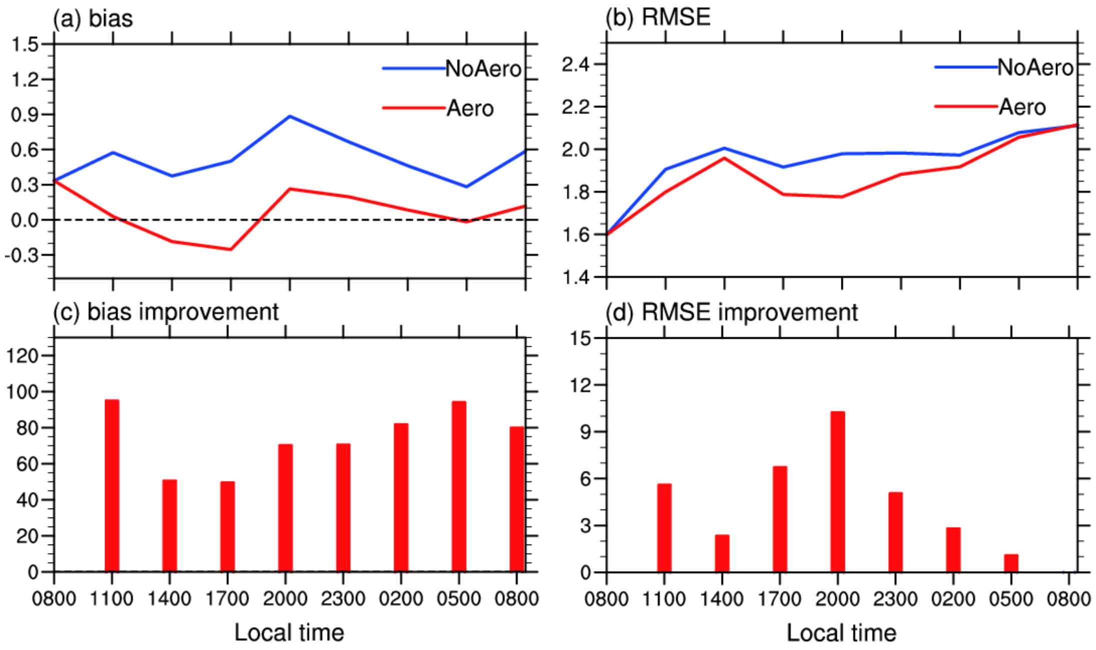

Figure 12. Area-averaged (a) bias and (b) RMSE of simulated 2-m temperature (°C) in NoAero (blue) and Aero (red) over NCP area (defined in Fig. 1a), averaged from 6th to 10th Dec. 2015, and the mean improvement (%) of (c) absolute value of bias and (d) RMSE in Aero relative to NoAero.

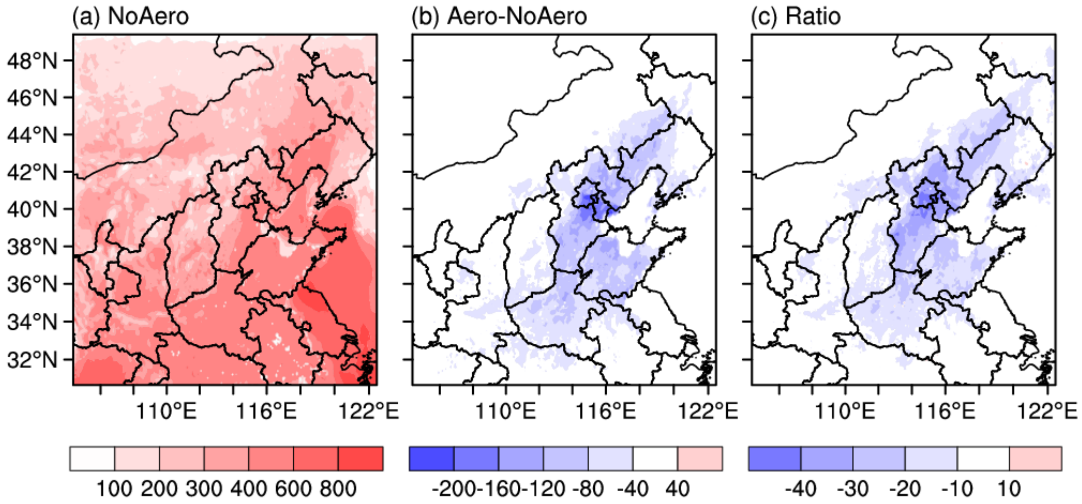

Figure 13. Daytime mean PBLH (m) in NoAero, (b) the difference between Aero and NoAero (Aero minus NoAero) and (c) the ratio of changes (%) averaged during 6th to 10th Dec. 2015.

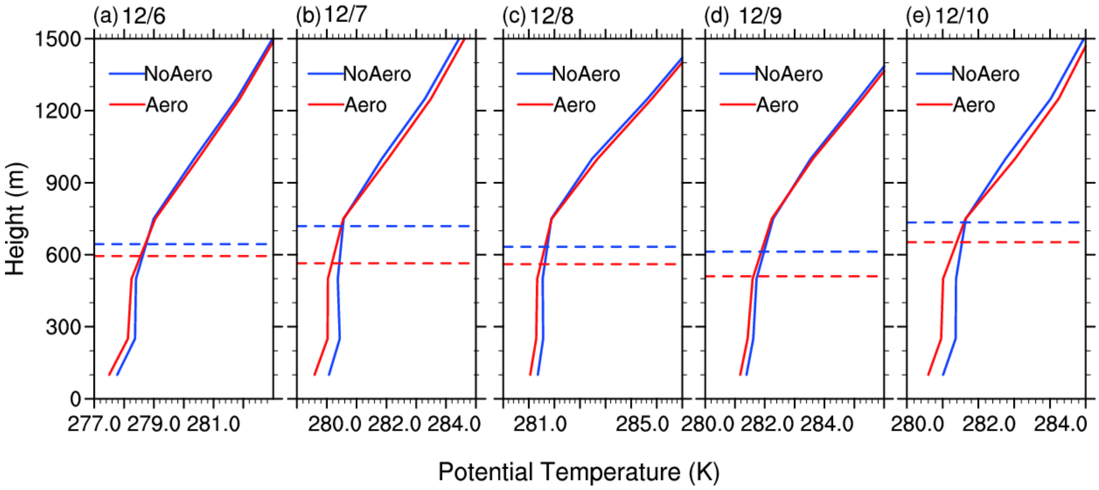

Figure 14. NCP (defined in Fig. 1a) area-averaged vertical profiles of potential temperature (K, solid) and planetary boundary-layer height (m, dash) in NoAero (blue) and Aero (red) at 1400 LT of (a) 6th, (b) 7th, (c) 8th, (d) 9th and (e) 10th Dec. 2015.

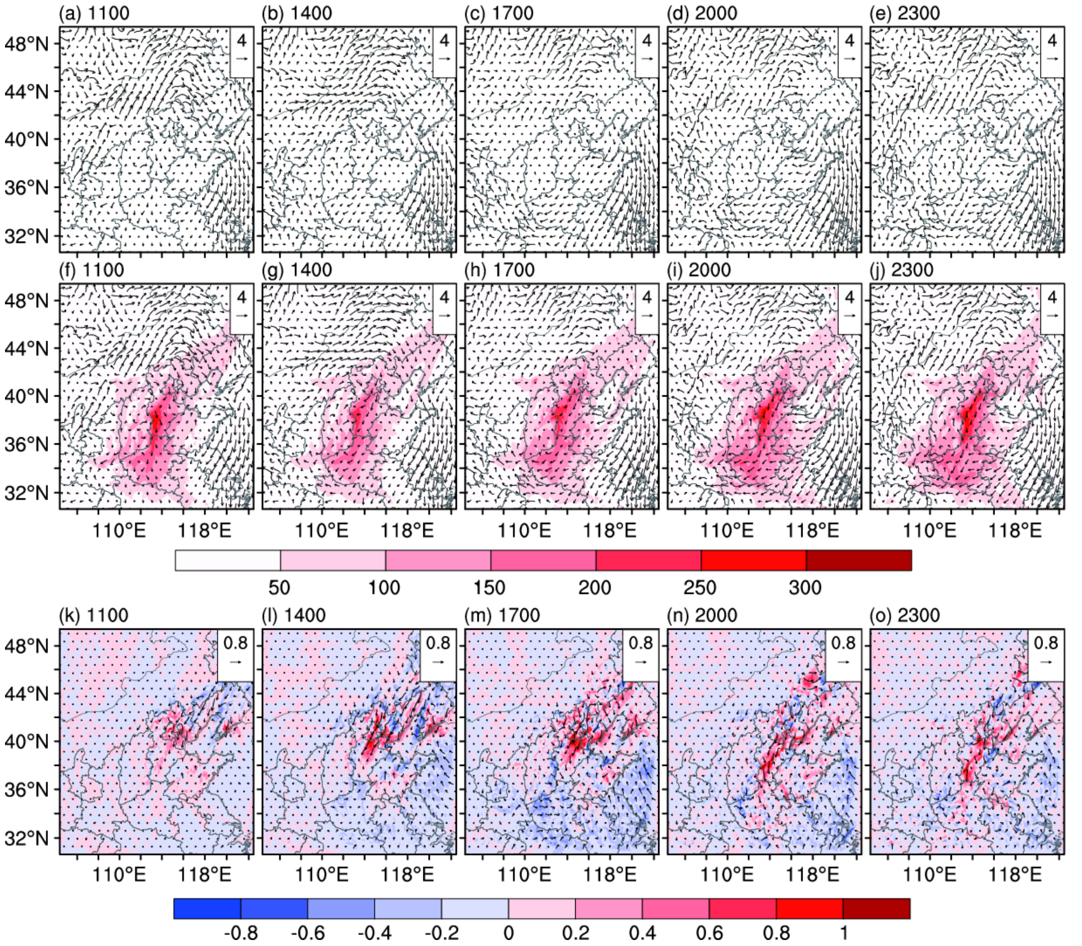

Figure 15. The 10m wind (vector) at 1100, 1400, 1700, 2000 and 2300 LT in (a–e) NoAero and (f–j) Aero averaged during 6th to 10th Dec. 2015, shadings in (f–j) are simulated $PM_{2.5}$ concentrations (μg m^{-3}). (k–o) the difference of 10m wind (vector) and wind speed (shadings) between Aero and NoAero (Aero minus NoAero).

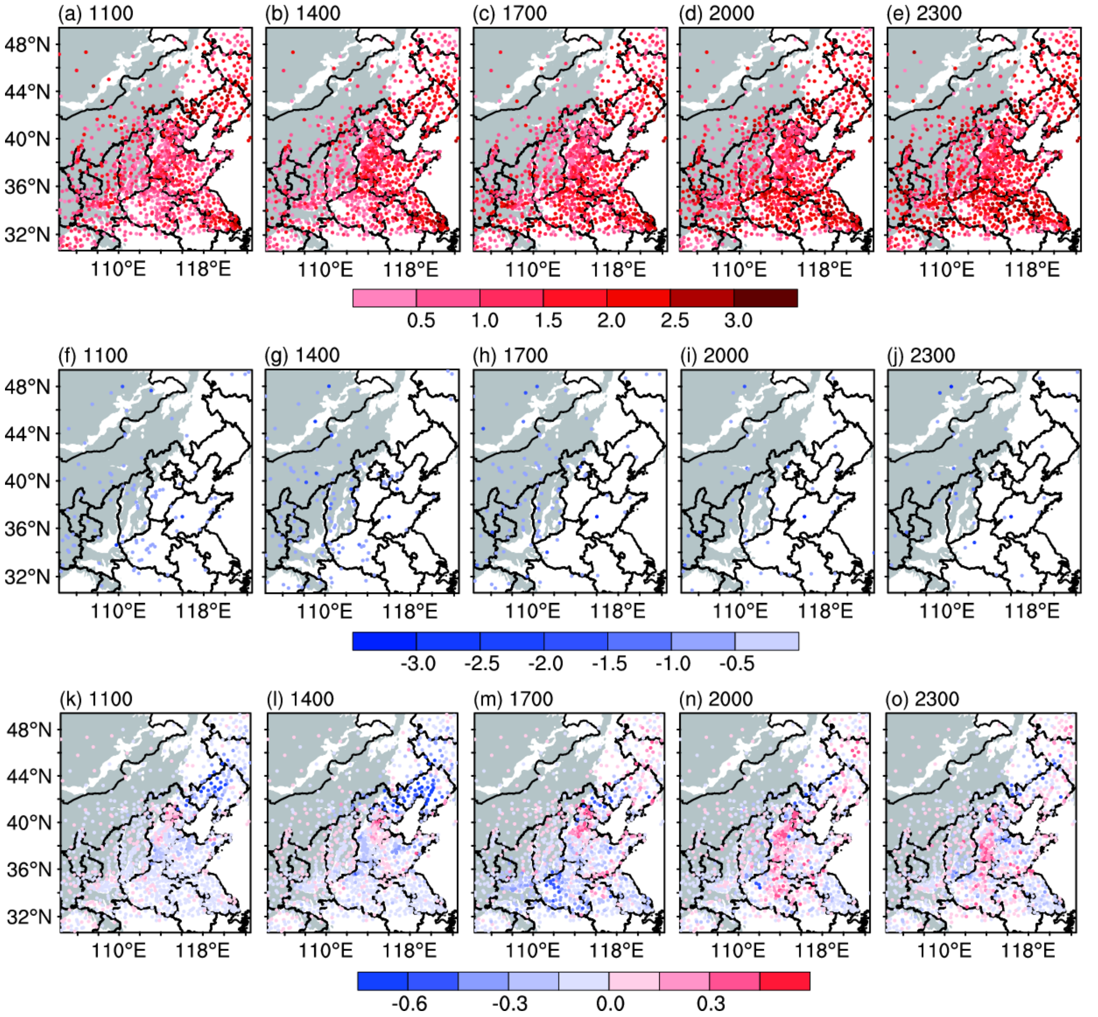

Figure 16. The bias of 10m wind speed (m s $^{-1}$) at 1100, 1400, 1700, 2000 and 2300 LT for (a–e) overestimated sites and (f–j) underestimated sites in NoAero averaged during 6th to 10th Dec. 2015. (k–o) the difference of absolute value of bias (m s $^{-1}$) between Aero and NoAero (Aero minus NoAero). The grey areas denote the areas of terrain height above 1000m.

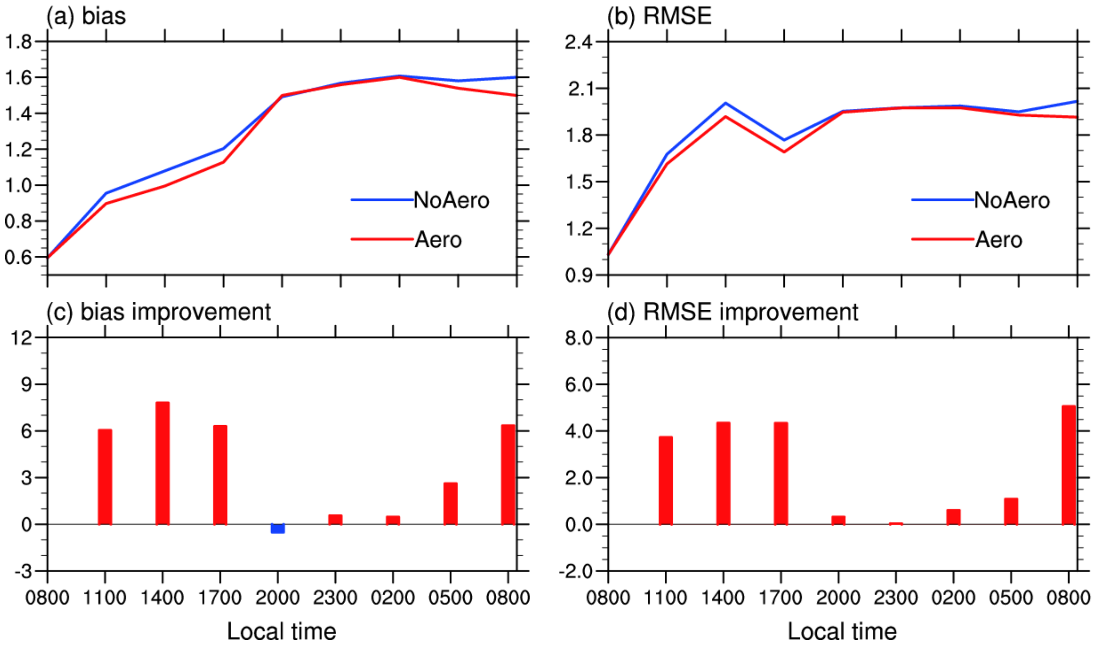

Figure 17. Same with Fig.12, but for wind speed at 10m (m s $^{-1}$).

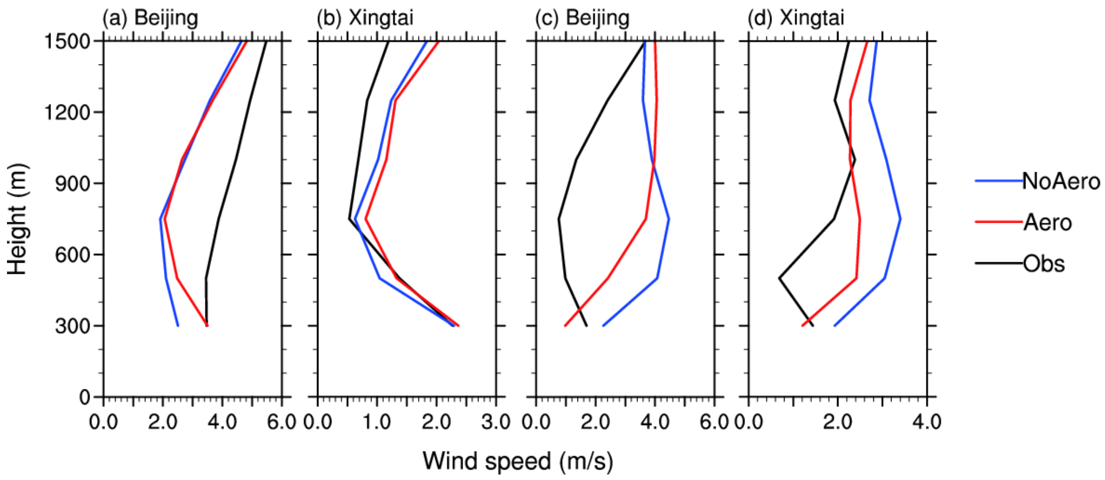

Figure 18. (a–b) Observed (black) and simulated (NoAero: blue, Aero: red) vertical profiles of atmospheric wind speed (m s $^{-1}$) at (a) Bejing and (b)Xingtai at 0800LT averaged from 6th to 10th Dec., (c–d) are same with (a–b), but at 2000LT.

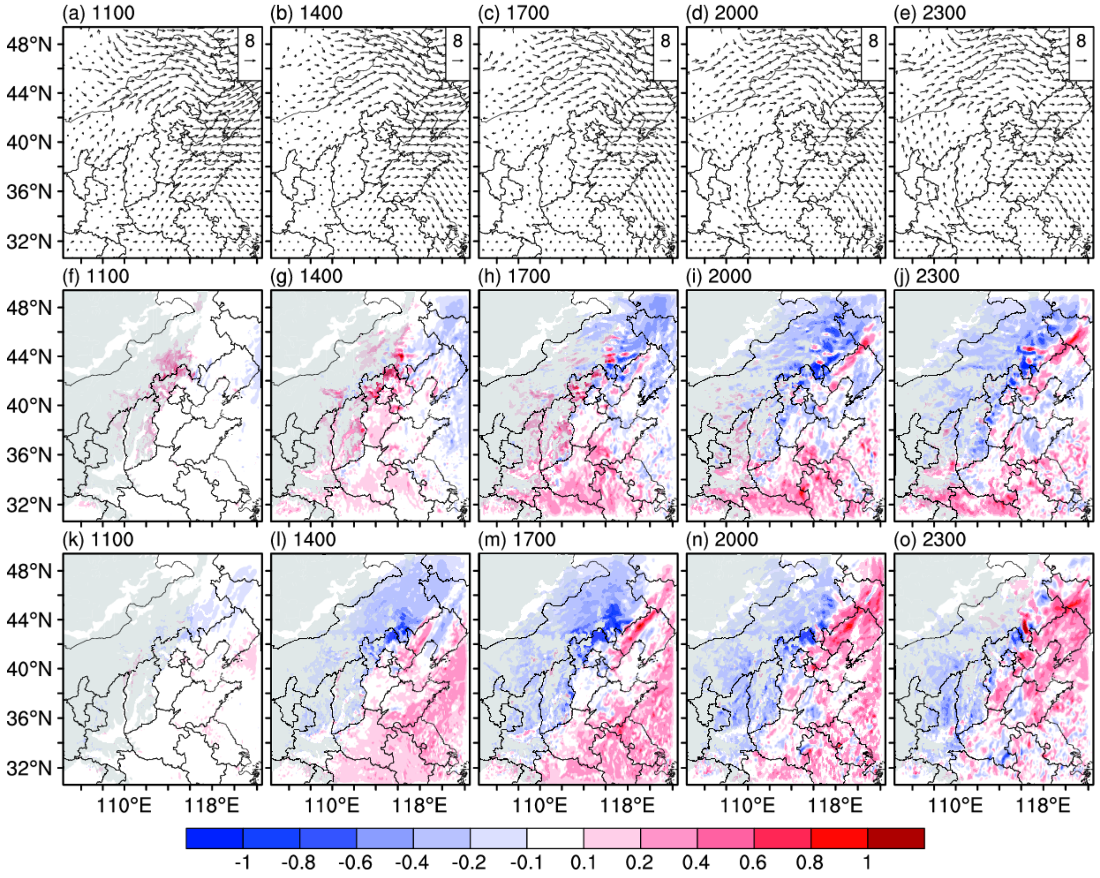

Figure 19. The wind at 850hPa (vector) at 1100, 1400, 1700, 2000 and 2300 LT in NoAero averaged during 6th to 10th Dec. 2015. The difference of (f–j) U and (k–o) V wind speed between Aero and NoAero (Aero minus NoAero). The grey areas denote the areas of terrain height above 1000m.